

Fig. 2. Inhibitory effects of chrysoeriol on BPDE-dG adduct formation in MCF-7 cells. Each adduct corresponded to the chromatogram in Fig. 1. Data are presented as the mean \pm SD ($n=3$). Statistical analysis for multiple comparison was performed using Tukey's test (** $P < 0.01$ versus group treated with BaP only). Closed bar, BaP treatment without chrysoeriol; slash lined bar, BaP and 5 μ M chrysoeriol treatment; dotted bar, BaP and 10 μ M chrysoeriol treatment.

3.3. Effects of chrysoeriol on CYP1 mRNA expression of BaP-treated MCF-7 cells

BaP treatment (2 μ M) of MCF-7 cells for 12 h resulted in significant increases in the CYP1A1, CYP1A2 and CYP1B1 mRNA levels which were approximately 80 ± 6.6 -, 17 ± 3.0 - and 5.8 ± 0.81 -fold higher than the vehicle control, respectively (Fig. 4). In the presence of chrysoeriol, all three CYP1 mRNA levels were inhibited in a dose-dependent manner. In particular, the expressions of CYP1A1 and 1A2 genes were significantly inhibited even at 1 μ M of chrysoeriol ($P < 0.05$), 5, 10 μ M of chrysoeriol ($P < 0.01$), respectively.

3.4. AhR antagonistic activity of chrysoeriol

We used the AhR-based bioassay in order to evaluate the influence of chrysoeriol on the AhR pathway stimulated by BaP. As shown in Fig. 5, chrysoeriol exhibited appreciable dose-dependent inhibition, ranging from 0.1 to 10 μ M when activated by 0.1 μ M of BaP treatment in this assay system. The inhibitory effects of chrysoeriol at 0.1, 1 and 10 μ M were significant, $56.6 \pm 9.1\%$, $37.3 \pm 6.3\%$ and $35.6 \pm 2.8\%$ ($P < 0.01$), respectively. On the other hand, chrysoeriol itself did not have any effects on AhR activation at concentrations of up to 10 μ M (data not shown).

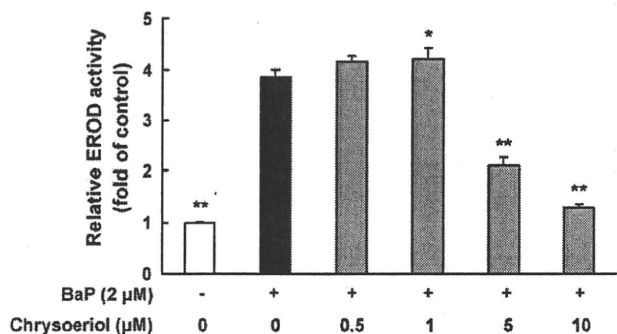


Fig. 3. Inhibitory effects of chrysoeriol on BaP-induced EROD activity in MCF-7 cells. Data are presented as the mean \pm SD ($n=4$). Statistical analysis for multiple comparison was performed using Tukey's test (* $P < 0.05$, ** $P < 0.01$ versus control group treated with BaP without chrysoeriol).

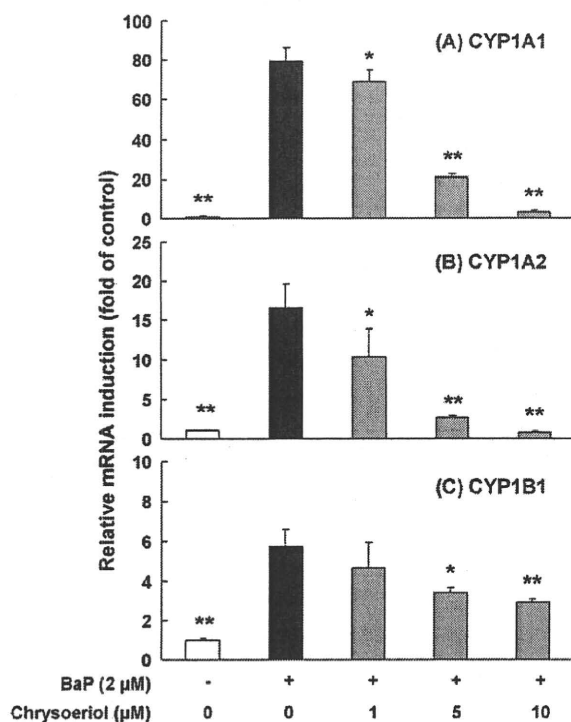


Fig. 4. Inhibitory effects of chrysoeriol on BaP-induced CYP1A1, CYP1A2 and CYP1B1 expression in MCF-7 cells. Data are presented as the mean \pm SD ($n=3$). Statistical analysis for multiple comparison was performed using Tukey's test (* $P < 0.05$, ** $P < 0.01$ versus control group treated with BaP without chrysoeriol).

4. Discussion

In the present study, we demonstrated that chrysoeriol had a preventive effect on stereoisomeric BPDE-dG formation in human MCF-7 breast cancer cells treated with BaP using the LC-MS/MS technique. When MCF-7 cells were incubated with 2 μ M of BaP for 24 h, three types of BPDE-dG adducts were detected. Predominant peak was identified as (+)-*trans*-BPDE-dG, because its retention time was confirmed to that of the standard compound used in our study. The (+)-*trans*-BPDE-dG was the dominant adduct in MCF-7 cells treated with BaP. This finding was consistent with two other studies which involved human bronchoalveolar H385 cells exposed to 2 μ M BaP or 2 μ M (\pm)-BaP-7,8-dihydroxydiol (Ruan et al., 2007) and human lung A549 cells exposed to 5 μ M

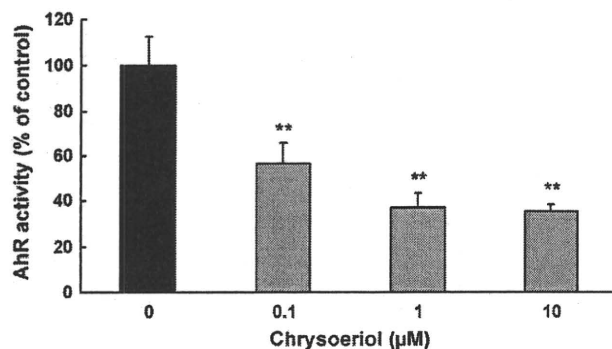


Fig. 5. Inhibitory effects of chrysoeriol on the AhR activation induced by BaP. The values obtained with BaP alone were considered to be 100% of the control value. Data are presented as the mean \pm SD ($n=3$). Statistical analysis for multiple comparison was performed using Tukey's test (** $P < 0.01$ versus vehicle controls treated with BaP alone).

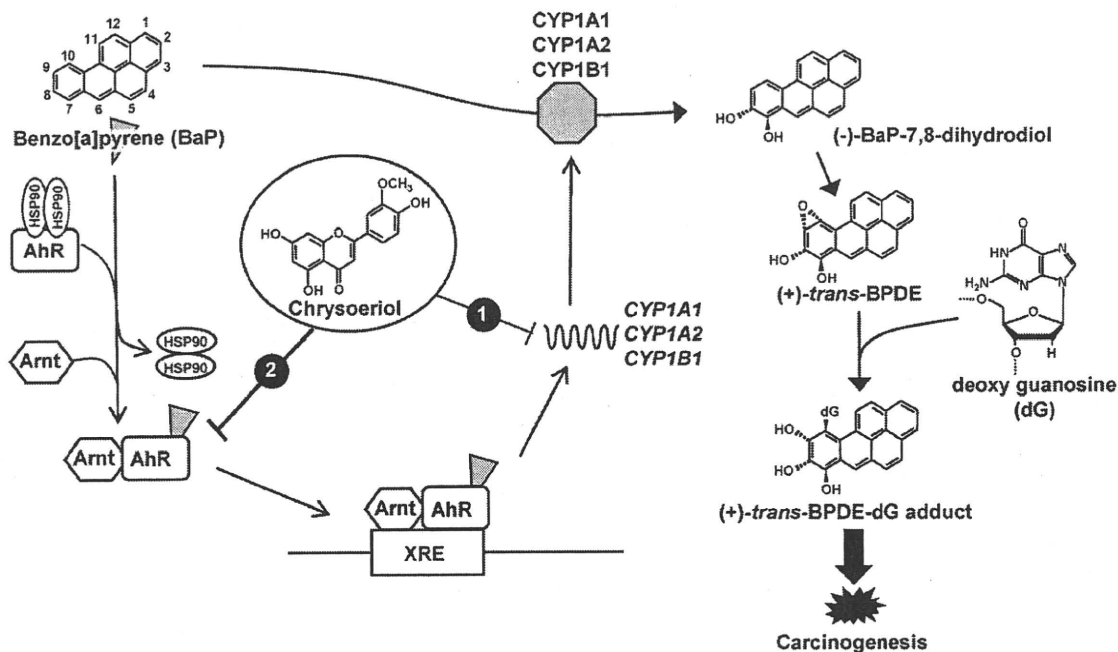


Fig. 6. Putative inhibitory mechanisms of chrysoeriol on BPDE-dG adduct formations in MCF-7 cells. HSP90, heat shock protein 90; AhR, arylhydrocarbon receptor; Arnt, AhR nuclear translocator; XRE, xenobiotic responsive element; BPDE, BaP-7,8-diol-9,10-epoxide (BPDE).

BaP (Feng et al., 2009). The (+)-*trans*-BPDE-dG adducts from (-)-BaP-7,8-dihydrodiol were detected in approximately twice the amount observed for (\pm)-BaP-7,8-dihydroxydiol-exposed H385 cells. In contrast, (+)-*trans*-BPDE-dG was not observed in (+)-BaP-7,8-dihydroxydiol-exposed cells. Therefore, the major adduct was (+)-*trans*-BPDE-dG, which means that the (-)-BaP-7,8-dihydrodiol-derived metabolite (+)-*anti*-BPDE was mainly responsible for DNA adduct formation (Cheng et al., 1989; Geacintov et al., 1997; Ruan et al., 2007). Three BPDE-dG adducts, in which (+)-*trans*-BPDE-dG was dominant and (+)-*cis*-BPDE-dG and *syn*-BPDE-dG were minors, were detected in A549 cells and H358 cells treated with BaP (Ruan et al., 2007; Feng et al., 2009), although four adducts appeared in A549 cells treated with BPDE (Feng et al., 2009). Hence, in common with human A549 lung cells and human bronchoalveolar H358 cells our results indicated that human MCF-7 breast cancer cells treated with BaP also generated three BPDE-dG adducts. Additionally, with the exception of (+)-*trans*-BPDE-dG, other peaks in our results could not be precisely identified. However, it was considered that peak 1 might be (+)-*cis*-BPDE-dG, and peak 2 might be *syn*-BPDE-dG, as referred to in previous reports (Ruan et al., 2007; Feng et al., 2008, 2009). Further studies are needed for the identification of these two adducts.

Co-treatment involving 1–10 μ M chrysoeriol in combination with BaP inhibited the sum total formation of BPDE-dG adducts in MCF-7 cells in a dose-dependant manner (Fig. 2). In particular, among the three adducts (+)-*trans*-BPDE-dG formation was incredibly diminished in the presence of chrysoeriol. (+)-*trans*-BPDE-dG is considered to be highly mutagenic in mammalian cells (Fernandes et al., 1998; Huang et al., 2003) and to be responsible for the observed tumorigenic effects in mouse skin (Levin et al., 1977) and mouse lung (Buening et al., 1978). Therefore, our results clearly indicate that chrysoeriol might be an effective food ingredient that could prevent DNA adduct formation with pro-carcinogens such as BaP. Chrysoeriol also inhibited the formation of Peak 1 ((+)-*cis*-BPDE-dG generated in MCF-7 cells by treatment with BaP) but did not inhibit the formation of Peak 2 (*syn*-BPDE-dG). Human breast cells are also known to express the other CYP families, such as CYP2C6, 2D6, 2E1, 3A4 and 3A5 (Williams

and Phillips, 2000). CYP3A5 catalyzes the metabolism of (-)-BaP-7,8-dihydrodiol to (+)-*anti*-BPDE (Roberts-Thomson et al., 1993), whereas little is known about the stereoselective metabolism of BaP-7,8-dihydrodiol by the other CYPs. *syn*-BPDE-dG might be produced by the other CYPs that are present in breast cells.

We further extended the investigation in order to elucidate the mechanisms involved in the prevention of BPDE-dG formation by chrysoeriol. BaP itself is not a mutagenic or carcinogenic compound until bioactivated by xenobiotic-metabolizing enzymes such as those in the CYP1 family and epoxide hydrolase (Conney, 1982; Pelkonen and Nebert, 1982; Hecht, 2002; Shimada, 2006). Additionally, of special note in relation to the CYP1 family and BaP is that BaP itself induces CYP1s (Nebert et al., 2000, 2004). Chrysoeriol clearly inhibited BaP-induced EROD activity in MCF-7 cells by roughly the same magnitude as observed in the experiment above (Fig. 3). Moreover, chrysoeriol significantly inhibited the gene expression of individual CYP1A1, 1A2 and 1B1 mRNA stimulated by BaP in MCF-7 cells (Fig. 4). It is well recognized that the expression of the CYP1 family genes are regulated by AhR, a ligand activated transcription factor (Whitlock, 1999; Nebert et al., 2004). Hence, in the final part of our study, using an AhR-based bioassay, we evaluated the antagonistic activity of chrysoeriol against BaP-induced activation of AhR. We found that BaP powerfully stimulated AhR activity, but the co-existence of chrysoeriol diminished this stimulation in a dose-dependent manner (Fig. 5). Many researchers have demonstrated the AhR antagonistic activities of substituted 3'-methoxyflavones in MCF-7 cells (Lu et al., 1995), human MCF-10A breast epithelial cells (Reiners et al., 1998) and mouse Hepa-1c1c7 hepatoma cells (Gasiewicz et al., 1996; Henry et al., 1999). In addition, 3',4'-methoxyflavone inhibited both AhR-mediated CYP1A1 induction and antiestrogenic activity in both MCF-7 and T47D breast cancer cell lines by blocking the transformation of the cytosolic AhR complex and the formation of the nuclear AhR complex (Lee and Safe, 2000). In the present study, chrysoeriol exhibited inhibitory effects on the formation of BPDE-dG adducts *via* the regulation of the AhR pathway, including activation of the CYP1 family stimulated by BaP. This finding indicated that 3'-methoxy-substituted flavones such as chrysoeriol might be potent AhR antagonists in breast cancer cells.

In conclusion, the present study is the first to report to demonstrate that chrysoeriol has preventive effects on BPDE-dG adduct formation in MCF-7 cells treated with BaP and evaluated using the LC-MS/MS technique. As shown in Fig. 6, pro-carcinogen BaP activates AhR pathway, and induces CYP1A1, 1A2 and 1B1 expression. Furthermore, BaP itself is metabolized to BPDE, mainly (+)-*trans*-BPDE, by induced CYP1s. Following, BPDE reacts with deoxyguanosine (dG), and forms BPDE-dG adducts, in which (+)-*trans*-BPDE-dG is dominant. In this study, the formation of (+)-*trans*-BPDE-dG was dramatically diminished by a 10 μ M concentration of chrysoeriol. One of the inhibitory mechanisms is considered as inhibition of CYP1s' gene expressions (Fig. 6, pathway 1), via blocking the formation of the AhR-BaP complex (Fig. 6, pathway 2). As a consequence, chrysoeriol may be involved in the chemoprevention of environmental pro-carcinogens such as BaP.

Conflict of interest statement

The authors declare that there are no conflicts of interest.

Acknowledgments

This work was supported partly by a Grant-in-Aid for Young Scientists (B) (20700601) from the Ministry of Education, Culture, Sports, Science and Technology of Japan. Additional funding was provided by the Global COE Program, the Center of Excellence for Innovation in Human Health Sciences, from the Ministry of Education, Science, and Culture of Japan.

References

- Amakura, Y., Tsutsumi, T., Sasaki, K., Yoshida, T., Maitani, T., 2003. Screening of the inhibitory effect of vegetable constituents on the aryl hydrocarbon receptor-mediated activity induced by 2,3,7,8-tetrachlorodibenzo-p-dioxin. *Biol. Pharm. Bull.* 26, 1754–1760.
- Boffetta, P., Jourenkova, N., Gustavsson, P., 1997. Cancer risk from occupational and environmental exposure to polycyclic aromatic hydrocarbons. *Cancer Causes Control* 8, 444–472.
- Buening, M.K., Wislocki, P.G., Levin, W., Yagi, H., Thakker, D.R., Akagi, H., Koreeda, M., Jerina, D.M., Conney, A.H., 1978. Tumorigenicity of the optical enantiomers of the diastereomeric benzo[a]pyrene 7,8-diol-9,10-epoxides in newborn mice: exceptional activity of (+)-7beta,8alpha-dihydroxy-9alpha,10alpha-epoxy-7,8,9,10-tetrahydrobenzo[a]pyrene. *Proc. Natl. Acad. Sci. U.S.A.* 75, 5358–5361.
- Cavaliere, E.L., Higginbotham, S., RamaKrishna, N.V., Devanesan, P.D., Todorovic, R., Rogan, E.G., Salmasi, S., 1991. Comparative dose-response tumorigenicity studies of dibenzo[alpha,]pyrene versus 7,12-dimethylbenz[alpha]anthracene, benzo[alpha]pyrene and two dibenzo[alpha,]pyrene dihydrodiols in mouse skin and rat mammary gland. *Carcinogenesis* 12, 1939–1944.
- Chang, R.L., Wood, A.W., Conney, A.H., Yagi, H., Sayer, J.M., Thakker, D.R., Jerina, D.M., Levin, W., 1987. Role of diaxial versus diequatorial hydroxyl groups in the tumorigenic activity of a benzo[a]pyrene bay-region diol epoxide. *Proc. Natl. Acad. Sci. U.S.A.* 84, 8633–8636.
- Cheng, S.C., Hilton, B.D., Roman, J.M., Dipple, A., 1989. DNA adducts from carcinogenic and noncarcinogenic enantiomers of benzo[a]pyrene dihydrodiol epoxide. *Chem. Res. Toxicol.* 2, 334–340.
- Choi, D.Y., Lee, J.Y., Kim, M.R., Woo, E.R., Kim, Y.G., Kang, K.W., 2005. Chrysoeriol potently inhibits the induction of nitric oxide synthase by blocking AP-1 activation. *J. Biomed. Sci.* 12, 949–959.
- Ciollino, H.P., Yeh, G.C., 1999. Inhibition of aryl hydrocarbon-induced cytochrome P-450 1A1 enzyme activity and CYP1A1 expression by resveratrol. *Mol. Pharmacol.* 56, 760–767.
- Conney, A.H., 1982. Induction of microsomal enzymes by foreign chemicals and carcinogenesis by polycyclic aromatic hydrocarbons: G. H. A. Clowes Memorial Lecture. *Cancer Res.* 42, 4875–4917.
- Dong, H., Bonala, R.R., Suzuki, N., Johnson, F., Grollman, A.P., Shibutani, S., 2004. Mutagenic potential of benzo[a]pyrene-derived DNA adducts positioned in codon 273 of the human P53 gene. *Biochemistry (Mosc.)* 43, 15922–15928.
- el-Bayoumy, K., Chae, Y.H., Upadhyaya, P., Rivenson, A., Kurtzke, C., Reddy, B., Hecht, S.S., 1995. Comparative tumorigenicity of benzo[a]pyrene, 1-nitropyrene and 2-amino-1-methyl-6-phenylimidazo[4,5-b]pyridine administered by gavage to female CD rats. *Carcinogenesis* 16, 431–434.
- Feng, F., Wang, X., Yuan, H., Wang, H., 2009. Ultra-performance liquid chromatography-tandem mass spectrometry for rapid and highly sensitive analysis of stereoisomers of benzo[a]pyrene diol epoxide-DNA adducts. *J. Chromatogr. B: Anal. Technol. Biomed. Life Sci.* 877, 2104–2112.
- Feng, F., Yin, J., Song, M., Wang, H., 2008. Preparation, identification and analysis of stereoisomeric anti-benzo[a]pyrene diol epoxide-deoxyguanosine adducts using phenyl liquid chromatography with diode array, fluorescence and tandem mass spectrometry detection. *J. Chromatogr. A* 1183, 119–128.
- Fernandes, A., Liu, T., Amin, S., Geacintov, N.E., Grollman, A.P., Moriya, M., 1998. Mutagenic potential of stereoisomeric bay region (+)- and (–)-*cis*-anti-benzo[a]pyrene diol epoxide-N2-2'-deoxyguanosine adducts in *Escherichia coli* and simian kidney cells. *Biochemistry (Mosc.)* 37, 10164–10172.
- Gammon, M.D., Sagiv, S.K., Eng, S.M., Shantakumar, S., Gaudet, M.M., Teitelbaum, S.L., Britton, J.A., Terry, M.B., Wang, L.W., Wang, Q., Stellman, S.D., Beyea, J., Hatch, M., Kabat, G.C., Wolff, M.S., Levin, B., Neugut, A.I., Santella, R.M., 2004. Polycyclic aromatic hydrocarbon-DNA adducts and breast cancer: a pooled analysis. *Arch. Environ. Health* 59, 640–649.
- Gasiewicz, T.A., Kende, A.S., Rucci, G., Whitney, B., Willey, J.J., 1996. Analysis of structural requirements for Ah receptor antagonist activity: ellipticines, flavones, and related compounds. *Biochem. Pharmacol.* 52, 1787–1803.
- Geacintov, N.E., Cosman, M., Hingerty, B.E., Amin, S., Broyde, S., Patel, D.J., 1997. NMR solution structures of stereoisomeric covalent polycyclic aromatic carcinogen-DNA adduct: principles, patterns, and diversity. *Chem. Res. Toxicol.* 10, 111–146.
- Grollman, A.P., Shibutani, S., 1994. Mutagenic specificity of chemical carcinogens as determined by studies of single DNA adducts. *IARC Sci. Publ.*, 385–397.
- Hecht, S.S., 2002. Tobacco smoke carcinogens and breast cancer. *Environ. Mol. Mutagen.* 39, 119–126.
- Henry, E.C., Kende, A.S., Rucci, G., Totleben, M.J., Willey, J.J., Dertinger, S.D., Pollenz, R.S., Jones, J.P., Gasiewicz, T.A., 1999. Flavone antagonists bind competitively with 2,3,7,8-tetrachlorodibenzo-p-dioxin (TCDD) to the aryl hydrocarbon receptor but inhibit nuclear uptake and transformation. *Mol. Pharmacol.* 55, 716–725.
- Huang, X., Kolbanovskiy, A., Wu, X., Zhang, Y., Wang, Z., Zhuang, P., Amin, S., Geacintov, N.E., 2003. Effects of base sequence context on translesion synthesis past a bulky (+)-*trans*-anti-B[a]P-N2-dG lesion catalyzed by the Y-family polymerase pol kappa. *Biochemistry (Mosc.)* 42, 2456–2466.
- Kapitulnik, J., Levin, W., Conney, A.H., Yagi, H., Jerina, D.M., 1977. Benzo[a]pyrene 7,8-dihydrodiol is more carcinogenic than benzo[a]pyrene in newborn mice. *Nature* 266, 378–380.
- Kapitulnik, J., Wislocki, P.G., Levin, W., Yagi, H., Jerina, D.M., Conney, A.H., 1978. Tumorigenicity studies with diol-epoxides of benzo(a)pyrene which indicate that (±)-*trans*-7beta,8alpha-dihydroxy-9alpha,10alpha-epoxy-7,8,9,10-tetrahydrobenzo(a)pyrene is an ultimate carcinogen in newborn mice. *Cancer Res.* 38, 354–358.
- Khan, A.U., Gilani, A.H., 2006. Selective bronchodilatory effect of Rooibos tea (*Aspalathus linearis*) and its flavonoid, chrysoeriol. *Eur. J. Nutr.* 45, 463–469.
- Lee, J.E., Safe, S., 2000. 3',4'-Dimethoxyflavone as an aryl hydrocarbon receptor antagonist in human breast cancer cells. *Toxicol. Sci.* 58, 235–242.
- Levin, W., Wood, A.W., Chang, R.L., Slaga, T.J., Yagi, H., Jerina, D.M., Conney, A.H., 1977. Marked differences in the tumor-initiating activity of optically pure (+) and (–)-*trans*-7,8-dihydroxy-7,8-dihydrobenzo(a)pyrene on mouse skin. *Cancer Res.* 37, 2721–2725.
- Lin, L.Z., Lu, S., Harnly, J.M., 2007. Detection and quantification of glycosylated flavonoid malonates in celery, Chinese celery, and celery seed by LC-DAD-ESI/MS. *J. Agric. Food Chem.* 55, 1321–1326.
- Lu, Y.F., Santostefano, M., Cunningham, B.D., Threadgill, M.D., Safe, S., 1995. Identification of 3'-methoxy-4'-nitroflavone as a pure aryl hydrocarbon (Ah) receptor antagonist and evidence for more than one form of the nuclear Ah receptor in MCF-7 human breast cancer cells. *Arch. Biochem. Biophys.* 316, 470–477.
- Nebert, D.W., Dalton, T.P., Okey, A.B., Gonzalez, F.J., 2004. Role of aryl hydrocarbon receptor-mediated induction of the CYP1 enzymes in environmental toxicity and cancer. *J. Biol. Chem.* 279, 23847–23850.
- Nebert, D.W., Roe, A.L., Dieter, M.Z., Solis, W.A., Yang, Y., Dalton, T.P., 2000. Role of the aromatic hydrocarbon receptor and [Ah] gene battery in the oxidative stress response, cell cycle control, and apoptosis. *Biochem. Pharmacol.* 59, 65–85.
- Ohura, T., Morita, M., Kuruto-Niwa, R., Amagai, T., Sakakibara, H., Shimoi, K., 2010. Differential action of chlorinated polycyclic aromatic hydrocarbons on aryl hydrocarbon receptor-mediated signaling in breast cancer cells. *Environ. Toxicol.* 25, 180–187.
- Pelkonen, O., Nebert, D.W., 1982. Metabolism of polycyclic aromatic hydrocarbons: etiologic role in carcinogenesis. *Pharmacol. Rev.* 34, 189–222.
- Ravanat, J.L., Douki, T., Duez, P., Gremaud, E., Herbert, K., Hofer, T., Lasserre, L., Saint-Pierre, C., Favier, A., Cadet, J., 2002. Cellular background level of 8-oxo-7,8-dihydro-2'-deoxyguanosine: an isotope based method to evaluate artefactual oxidation of DNA during its extraction and subsequent work-up. *Carcinogenesis* 23, 1911–1918.
- Reiners Jr., J.J., Lee, J.Y., Clift, R.E., Dudley, D.T., Myrand, S.P., 1998. PD98059 is an equipotent antagonist of the aryl hydrocarbon receptor and inhibitor of mitogen-activated protein kinase. *Mol. Pharmacol.* 53, 438–445.
- Roberts-Thomson, S.J., McManus, M.E., Tukey, R.H., Gonzalez, F.F., Holder, G.M., 1993. The catalytic activity of four expressed human cytochrome P450s towards benzo[a]pyrene and the isomers of its proximate carcinogen. *Biochem. Biophys. Res. Commun.* 192, 1373–1379.
- Ruan, Q., Gelhaus, S.L., Penning, T.M., Harvey, R.G., Blair, I.A., 2007. Aldo-keto reductase- and cytochrome P450-dependent formation of benzo[a]pyrene-derived DNA adducts in human bronchoalveolar cells. *Chem. Res. Toxicol.* 20, 424–431.

- Shimada, T., 2006. Xenobiotic-metabolizing enzymes involved in activation and detoxification of carcinogenic polycyclic aromatic hydrocarbons. *Drug Metab. Pharmacokinet.* 21, 257–276.
- Shimada, T., Oda, Y., Gillam, E.M., Guengerich, F.P., Inoue, K., 2001. Metabolic activation of polycyclic aromatic hydrocarbons and other procarcinogens by cytochromes P450 1A1 and P450 1B1 allelic variants and other human cytochromes P450 in *Salmonella typhimurium* NM2009. *Drug Metab. Dispos.* 29, 1176–1182.
- Singh, R., Gaskell, M., Le Pla, R.C., Kaur, B., Azim-Araghi, A., Roach, J., Koukouves, G., Souliotis, V.L., Kyrtopoulos, S.A., Farmer, P.B., 2006. Detection and quantitation of benzo[a]pyrene-derived DNA adducts in mouse liver by liquid chromatography–tandem mass spectrometry: comparison with ³²P-postlabeling. *Chem. Res. Toxicol.* 19, 868–878.
- Snijman, P.W., Swanevelder, S., Joubert, E., Green, I.R., Gelderblom, W.C., 2007. The antimutagenic activity of the major flavonoids of Rooibos (*Aspalathus linearis*): some dose–response effects on mutagen activation–flavonoid interactions. *Mutat. Res.* 631, 111–123.
- Sundberg, K., Dreij, K., Seidel, A., Jernstrom, B., 2002. Glutathione conjugation and DNA adduct formation of dibenzo[a,h]pyrene and benzo[a]pyrene diol epoxides in V79 cells stably expressing different human glutathione transferases. *Chem. Res. Toxicol.* 15, 170–179.
- Suzuki, N., Ohashi, E., Kolbanovskiy, A., Geacintov, N.E., Grollman, A.P., Ohmori, H., Shibutani, S., 2002. Translesion synthesis by human DNA polymerase kappa on a DNA template containing a single stereoisomer of dG-(+)- or dG-(-)-anti-N(2)-BPDE (7,8-dihydroxy-anti-9,10-epoxy-7,8,9,10-tetrahydrobenzo[a]pyrene). *Biochemistry (Mosc.)* 41, 6100–6106.
- Takemura, H., Uchiyama, H., Ohura, T., Sakakibara, H., Kuruto, R., Amagai, T., Shimoi, K., 2010. A methoxyflavonoid, chrysoeriol, selectively inhibits the formation of a carcinogenic estrogen metabolite in MCF-7 breast cancer cells. *J. Steroid Biochem. Mol. Biol.* 118, 70–76.
- Terashima, I., Suzuki, N., Shibutani, S., 2002. ³²P-Postlabeling/polyacrylamide gel electrophoresis analysis: application to the detection of DNA adducts. *Chem. Res. Toxicol.* 15, 305–311.
- Whitlock Jr., J.P., 1999. Induction of cytochrome P4501A1. *Annu. Rev. Pharmacol. Toxicol.* 39, 103–125.
- Williams, J.A., Phillips, D.H., 2000. Mammary expression of xenobiotic metabolizing enzymes and their potential role in breast cancer. *Cancer Res.* 60, 4667–4677.

Lipid Peroxidation Generates Body Odor Component *trans*-2-Nonenal Covalently Bound to Protein *in Vivo*^{*[5]}

Received for publication, September 22, 2009, and in revised form, March 7, 2010. Published, JBC Papers in Press, March 8, 2010, DOI 10.1074/jbc.M109.068023

Kousuke Ishino[‡], Chika Wakita[‡], Takahiro Shibata[‡], Shinya Toyokuni[§], Sachiko Machida[¶], Shun Matsuda^{||}, Tomonari Matsuda^{||}, and Koji Uchida^{†1}

From the [‡]Graduate School of Bioagricultural Sciences, Nagoya University, Nagoya 464-8601, the [§]Department of Pathology and Biological Responses, Graduate School of Medicine, Nagoya University, Nagoya 466-8550, the [¶]National Food Research Institute, 2-1-12 Kannondai, Tsukuba, Ibaraki 305-8642, and the ^{||}Research Center for Environmental Quality Management, Kyoto University, 1-2 Otsu, 520-0811, Japan

trans-2-Nonenal is an unsaturated aldehyde with an unpleasant greasy and grassy odor endogenously generated during the peroxidation of polyunsaturated fatty acids. 2-Nonenal covalently modified human serum albumin through a reaction in which the aldehyde preferentially reacted with the lysine residues. Modified proteins were immunogenic, and a specific monoclonal antibody (mAb) 27Q4 that cross-reacted with the protein covalently modified with 2-nonenal was raised from mouse. To verify the presence of the protein-bound 2-nonenal *in vivo*, the mAb 27Q4 against the 2-nonenal-modified keyhole limpet hemocyanin was raised. It was found that a novel 2-nonenal-lysine adduct, *cis*- and *trans*-*N*^ε-3-[(hept-1-enyl)-4-hexylpyridinium]lysine (HHP-lysine), constitutes an epitope of the antibody. The immunoreactive materials with mAb 27Q4 were detected in the kidney of rats exposed to ferric nitrilotriacetate, an iron chelate that induces free radical-mediated oxidative tissue damage. Using high performance liquid chromatography with on-line electrospray ionization tandem mass spectrometry, we also established a highly sensitive method for detection of the *cis*- and *trans*-HHP-lysine and confirmed that the 2-nonenal-lysine adducts were indeed formed during the lipid peroxidation-mediated modification of protein *in vitro* and *in vivo*. Furthermore, we examined the involvement of the scavenger receptor lectin-like oxidized low density lipoprotein receptor-1 in the recognition of 2-nonenal-modified proteins and established that the receptor recognized the HHP-lysine adducts as a ligand.

Lipid peroxidation in tissue and in tissue fractions represents a degradative process, which is the consequence of the production and propagation of free radical reactions primarily involving membrane polyunsaturated fatty acids, and has been implicated in the pathogenesis of numerous diseases, including atherosclerosis, diabetes, cancer, and rheumatoid arthritis, as well as in drug-associated toxicity, postischemic reoxygenation injury, and aging (1). The peroxidative breakdown of polyun-

saturated fatty acids has also been implicated in the pathogenesis of many types of liver injuries and especially in the hepatic damage induced by several toxic substances. The lipid peroxidation leads to the formation of a broad array of different products with diverse and powerful biological activities. Among them are a variety of different aldehydes (2). The primary products of lipid peroxidation, lipid hydroperoxides, can undergo carbon-carbon bond cleavage via alkoxyl radicals in the presence of transition metals giving rise to the formation of short-chain, unesterified aldehydes or a second class of aldehydes still esterified to the parent lipid. These reactive aldehydic intermediates readily form covalent adducts with cellular macromolecules, including protein, leading to the disruption of important cellular functions. The important agents that give rise to the modification of protein may be represented by α,β -unsaturated aldehydic intermediates, such as 2-alkenals, 4-hydroxy-2-alkenals, and 4-oxo-2-alkenals (3, 4).

2-Alkenals represent a group of highly reactive aldehydes containing two electrophilic reaction centers. A partially positive carbon 1 or 3 in such molecules can attack nucleophiles, such as protein. It has been suggested that these aldehydes primarily react with the sulfhydryl group of cysteine, the ϵ -amino group of lysine, and the imidazole group of histidine in the proteins (2, 3). Among the 2-alkenals, 2-nonenal (Fig. 1A) has a characteristically unpleasant greasy and grassy odor. It is also a major contributor to the unpleasant cardboard flavor in aged beer. It was previously shown that 2-nonenal could be formed through lipid peroxidation as a minor product in peroxide-mediated oxidation of high concentrations of linoleic acid hydroperoxide or from liver microsomes treated with ADP/iron *in vitro* (2). Toyokuni *et al.* (5) also reported the production of C2–C12 saturated and unsaturated aldehydes, including 2-nonenal, in the kidney of rats exposed to Fe³⁺-NTA.² More

² The abbreviations used are: Fe³⁺-NTA, ferric nitrilotriacetate; AcLDL, acetylated LDL; BSA, bovine serum albumin; DiD, 1,1'-dioctadecyl-3,3',3'-tetramethylindodicarbocyanine perchlorate; ELISA, enzyme-linked immunosorbent assay; HHP-lysine, *N*^ε-3-[(hept-1-enyl)-4-hexylpyridinium]lysine; HMBC, ¹H-detected multiple-bond connectivity; KLH, keyhole limpet hemocyanin; LDL, low density lipoprotein; LOX-1, lectin-like oxidized LDL receptor; HSA, human serum albumin; LC/ESI/MS/MS, high performance liquid chromatography with on-line electrospray ionization tandem mass spectrometry; mAb, monoclonal antibody; MRM, multiple reaction monitoring; PBS, phosphate-buffered saline; HPLC, high pressure liquid chromatography; CFP, cyan fluorescent protein; CHO, Chinese hamster ovary; Fmoc, *N*-(9-fluorenyl)methoxycarbonyl; HSA, human serum albumin.

* This work was supported by a grant-in-aid for scientific research on innovative areas (research in a proposed research area), from the Ministry of Education, Culture, Sports, Science and Technology, Japan (to K. U.).

[5] The on-line version of this article (available at <http://www.jbc.org>) contains supplemental Figs. S1–S22.

¹ To whom correspondence should be addressed. Fax: 81-52-789-5741; E-mail: uchidak@agr.nagoya-u.ac.jp.

recently, Haze *et al.* (6) analyzed the body odor components that adhered to the shirts of the subjects by gas chromatography/mass spectrometry and demonstrated that 2-nonenal is present in increasing amounts in the body odors of persons 40 years or older. They have also suggested that *cis*-2-nonenal and *trans*-2-nonenal are formed from the oxidative degradation of polyunsaturated fatty acids, such as palmitoleic acid. However, it is still not clear how 2-nonenal could be formed *in vivo*. Because of its insolubility in water, 2-nonenal is less reactive with proteins than other 2-alkenals, such as acrolein and crotonaldehyde, and therefore has received relatively little attention as a causative agent for modification of proteins. Only inhibition of enzymes, such as platelet membrane-bound phosphotyrosine phosphatase (7) and liver microsomal glucose-6-phosphatase (8), has been reported.

A structurally diverse protein supergroup called scavenger receptors mediates the cellular uptake of modified lipoproteins. Scavenger receptors are expressed by endothelial cells, macrophages, and smooth muscle cells and mediate recognition, internalization, and physiological responses to a wide range of ligands, including phospholipids, lipoprotein particles, apoptotic cells, and pathogens. Several oxidized low density lipoprotein (LDL) receptors have been identified so far, including SR-A I/II, CD36, SR-BI, Fc γ RII, lectin-like oxidized LDL receptor (LOX-1), macroscialin, SR expressed by endothelial cells, etc. Among them, LOX-1 is characterized as the major receptor for oxidized LDL in the endothelial cells of large arteries. Its inducible expression (9) might be involved in the oxidized LDL-mediated endothelial dysfunction. LOX-1 exhibits a binding activity for multiple ligands. LOX-1 is capable of interacting with a variety of structurally and functionally distinct ligands, including oxidized LDL, platelets, aged red blood cells, apoptotic cells, advanced glycation end products, heat shock protein 70, bacteria, and phosphatidylserine (10). LOX-1 binds and internalizes a diverse array of macromolecules, although their structures are not always related to each other.

In this study, to understand the mechanism underlying the formation of a covalently modified protein with 2-nonenal *in vivo*, we raised a monoclonal antibody (mAb) against protein-bound 2-nonenal and identified a novel 2-nonenal-lysine adduct as the epitope. Our immunohistochemical studies demonstrated the localization of the immunoreactive materials in the kidney of rats exposed to Fe³⁺-NTA, an iron chelate that induces acute renal proximal tubular necrosis, a consequence of free radical-mediated oxidative tissue damage, eventually leading to a high incidence of renal adenocarcinoma in rodents. Importantly, using high performance liquid chromatography with on-line electrospray ionization tandem mass spectrometry (LC/ESI/MS/MS), we also showed evidence that the 2-nonenal-lysine adduct is indeed accumulated during the lipid peroxidation-mediated modification of protein *in vitro* and *in vivo*. Furthermore, to evaluate the biological implication of the 2-nonenal modification of protein, we examined the involvement of LOX-1, a member of the scavenger receptor family, in the recognition of the 2-nonenal-lysine adducts.

EXPERIMENTAL PROCEDURES

Materials—*trans*-2-Nonenal (2-nonenal), *N*^α-acetyl-L-lysine, and human serum albumin (HSA) were obtained from the Sigma. Acrolein was obtained from Tokyokasei (Tokyo, Japan). *N*^α-[U-¹³C₆, ¹⁵N₂]Fmoc-*N*^ε-*boc*-lysine (where *boc* is *t*-butoxycarbonyl) was obtained from the Cambridge Isotope Laboratories (Andover, MA). The keyhole limpet hemocyanin (KLH) was obtained from Pierce. Ferric nitrate nonahydrate, sodium carbonate, and bovine serum albumin (BSA) were from Wako (Osaka, Japan), and the nitrilotriacetic acid disodium salt was from Nacalai Tesque, Inc. (Kyoto, Japan). The Fe³⁺-NTA solution was prepared immediately before use by the method described in a previous study (11). The stock solutions of 4-hydroxy-2-nonenal were prepared by the acid treatment (1 mM HCl) of 4-hydroxy-2-nonenal dimethyl acetal, which was synthesized according to the procedure of De Montarby *et al.* (12). 4-Oxo-2-nonenal was synthesized by the oxidation of 4-hydroxy-2-nonenal dimethyl acetal with pyridinium dichlorochromate, followed by HCl hydrolysis (13). The sodium salt of malondialdehyde was prepared by the Dowex hydrolysis of malondialdehyde bis(diethyl acetal) (14). Other aldehydes were purchased from Wako.

In Vitro Modification of HSA—Modification of the protein by 2-nonenal and its related short-chain aldehydes was performed by incubating HSA (1.0 mg/ml) with 0–10 mM 2-nonenal in 1 ml of 50 mM sodium phosphate buffer, pH 7.2, at 37 °C for 24 h. The Fe²⁺-catalyzed oxidation of unsaturated fatty acids in the presence of HSA was performed by incubating HSA (1 mg/ml) with 2 mM unsaturated fatty acids in the presence of 50 μM Fe²⁺ and 1 mM ascorbic acid in 1 ml of 50 mM sodium phosphate buffer, pH 7.2, in atmospheric oxygen at 37 °C. The reaction was terminated by the addition of 1 mM butylated hydroxytoluene and 100 μM diethylenetriaminepentaacetic acid.

In Vitro Peroxidation of LDL—LDL (1.019–1.063 g/ml) was prepared from the plasma of healthy humans by sequential ultracentrifugation and then extensively dialyzed three times against phosphate-buffered saline (PBS, 10 mM sodium phosphate buffer, pH 7.2, containing 150 mM NaCl) containing 0.01% EDTA at 4 °C. LDL used for the oxidative modification by Cu²⁺ was dialyzed five times against a 1000-fold volume of PBS at 4 °C. The oxidation of LDL was performed by incubating 0.5 mg of LDL with CuSO₄ (5 μM) in 1 ml of PBS for 24 h at 37 °C. The reaction was terminated by the addition of 1 mM EDTA and then stored at 4 °C.

Amino Acid Analysis—An aliquot (0.2 ml) of the protein samples (1 mg/ml) incubated for 24 h at 37 °C in the absence or presence of 2-nonenal was treated with 10 mM EDTA (20 μl), 1 N NaOH (20 μl), and 100 mM sodium borohydride (20 μl). After incubation for 1 h at room temperature, 20 μl of 2 N HCl was added to the mixture to stop the reaction, and the mixture was then incubated for 60 min at room temperature after adding 280 μl of 20% trichloroacetic acid. After centrifugation at 5,000 × *g* for 10 min at 4 °C, the proteins were hydrolyzed *in vacuo* with 2 ml of 6 N HCl for 24 h at 110 °C. The hydrolysates were then dried and dissolved in sodium citrate buffer, pH 3.15. The amino acid analysis was performed using a JEOL JLC-500

Lipid Peroxidation Generates Protein-bound 2-Nonenal

amino acid analyzer equipped with a JEOL LC30-DK20 data analyzing system.

Preparation of Monoclonal Antibody against 2-Nonenal-modified Protein—The immunogen was prepared by incubating the KLH (1.0 mg/ml) with 10 mM 2-nonenal in 3 ml of PBS at 37 °C for 24 h. We immunized the female BALB/c mice (Chubu Kagaku Shizai Co., Ltd., Nagoya, Japan) on day 1 with complete Freund adjuvant and 0.06 mg of immunogen (2-nonenal-modified KLH) and boosted on days 11, 21, and 31 with incomplete Freund adjuvant and 0.02 mg of immunogen by emulsifying and intraperitoneal injection. Titers to 2-nonenal-modified BSA in the immunized mice sera were measured by an enzyme-linked immunosorbent assay (ELISA) (15). Two months after the initial immunization, the immunized mice were given an intraperitoneal boost of 0.06 mg/ml 2-nonenal-modified KLH. Three days later, the spleen cells from the immunized mice were fused with P3/U1 murine myeloma cells in the presence of polyethylene glycol and cultured in hypoxanthine/amethopterin/thymidine selection medium. The culture supernatants of the hybridoma were screened using an ELISA, employing pairs of wells of microtiter plates on which were absorbed 2-nonenal-treated BSA as the antigen (0.5 µg of protein/well). After incubation with 100 µl of the hybridoma supernatants, and with intervening washes with PBS/Tween, the wells were incubated with alkaline phosphatase-conjugated goat anti-mouse IgG, followed by a substrate solution containing 0.5 mg/ml 1,2-phenylenediamine. Hybridoma cells corresponding to the supernatants that were positive on the 2-nonenal-modified BSA and negative on the native BSA were then cloned by limited dilution. After repeated screening, four clones were obtained. Among them, clone 27Q4 showed the most significant recognition of the 2-nonenal-modified BSA. Competitors were prepared by incubating 50 mM amino acid derivatives, *N*^α-acetyl-L-lysine, *N*^α-acetylhistidine, or *N*^α-acetylcysteine, in the presence or absence of 2-nonenal (50 mM), in 50 mM sodium phosphate buffer, pH 7.2, for 24 h at 37 °C.

Isolation and Structural Analysis of Antigenic 2-Nonenal-Lysine Adducts—The reaction mixture (6 ml) contained 200 mM *trans*-2-nonenal and 200 mM *N*^α-acetyl-L-lysine in 50 mM sodium phosphate buffer, pH 7.2. After incubation for 72 h at 37 °C, a portion of the reaction mixture was analyzed by a reverse-phase HPLC using a Develosil ODS-HG-5 column (4.6 × 250 mm, Nomura Chemicals) equilibrated in a solution of 5% acetonitrile in 0.01% trifluoroacetic acid. The chromatographic separation was performed by a gradient elution as follows (solvent A was water and solvent B was acetonitrile, both containing 0.01% trifluoroacetic acid): 0–10 min, linear gradient to 40% B; 10–40 min, 40% B; 40–41 min, linear gradient to 100% B; 41–45 min, hold; flow rate = 0.8 ml/min. The isolation and purification of the antigenic adducts (P-1 and P-2) were carried out under the same HPLC conditions and finally obtained 2.3 and 2.9 mg of P-1 and P-2, respectively. Their structures were characterized by LC/MS and ¹H and ¹³C NMR. The LC/MS was measured by a Jasco PlatformII-LC instrument. The LC/MS analysis was performed using a Develosil ODS-HG-5 column (4.6 × 250 mm) eluted with a linear gradient from 100% water containing 0.1% acetic acid to 100% acetonitrile containing 0.1% acetic acid for 60 min at a flow rate of

0.8 ml/min. The elution profiles were monitored by absorbance at 239 nm. The NMR analyses were performed using a Bruker AMX400 (400 MHz) instrument. For P-1, ¹H NMR (400 MHz, MeOD): δ 0.85–0.92 (6H, m), 1.25–1.50 (22H, m), 1.66 (2H, m), 1.70–2.08 (7H, m), 2.13 (2H, q), 2.87 (2H, t), 4.36 (1H, q), 4.55 (2H, t), 6.16 (1H, m), 6.51 (1H, d, *J* = 11.6 Hz), 7.93 (1H, d, *J* = 6.4 Hz), 8.66 (1H, s), and 8.70 (1H, d, *J* = 5.4 Hz). For P-2, ¹H NMR (MeOD, 600 MHz): δ 0.89–0.94 (6H, m), 1.30–1.52 (11H, m), 1.40–1.52 (2H, m), 1.56 (2H, m), 1.66 (2H, m), 1.70–1.92 (2H, m), 1.96 (3H, s), 2.01–2.06 (2H, m), 2.36 (2H, q), 2.93 (2H, t), 4.39 (1H, q), 4.53 (2H, q), 6.54 (1H, m), 6.66 (1H, d, *J* = 16.2 Hz), 7.84 (1H, d, *J* = 6.0 Hz), 8.61 (1H, d, *J* = 6.0 Hz), 8.91 (1H, s); ¹³C NMR (150 MHz, MeOD): δ 14.3 (2C), 22.4, 23.4, 23.5 (2C), 29.5, 30.0, 30.2, 31.6, 32.1, 32.5, 32.6, 34.0, 34.2, 53.0, 62.0, 122.4, 129.2, 139.4, 142.2 (2C), 142.5, 160.7, 173.3, and 175.1.

Immunohistochemical Detection of 2-Nonenal Adducts in Vivo—Male Wistar rats (Shizuoka Laboratory Animal Center, Shizuoka, Japan), weighing 130–150 g (6 weeks old), were used. The animals received a single intraperitoneal injection of Fe³⁺-NTA (15 mg of iron/kg of body weight) or repeated administration as described previously (5). They were sacrificed by decapitation at 0, 1, 6, 24, and 48 h after a single injection or 3 weeks after the repeated administration. Both kidneys of each animal were immediately removed. One of them was fixed in Bouin's solution, embedded in paraffin, cut in 3-mm thick slices, and used for the immunohistochemical analyses by an avidin-biotin complex method with alkaline phosphatase. Briefly, after deparaffinization with xylene and ethanol, normal rabbit serum (Dako; diluted to 1:75) for the inhibition of the nonspecific binding of the secondary antibody, a primary antibody (20 µg/ml), biotin-labeled rabbit anti-mouse IgG serum (Vector Laboratories; diluted to 1:300), and avidin-biotin complex (Vector; diluted to 1:100) were sequentially used. Procedures, using PBS or the IgG fraction (0.5 mg/ml) of the normal mouse serum instead of mAb 27Q4, showed no response or negligible positive responses.

Preparation of Isotope-labeled HPH-lysines—To prepare the [U-¹³C₆, ¹⁵N₂]HHP-lysine, 1 mM *N*^α-[U-¹³C₆, ¹⁵N₂]Fmoc-*N*^ε-Boc-lysine was treated with 1 ml of trifluoroacetic acid for 2 h at room temperature, applied to a C-18 Sep-Pak column, and eluted with 5 ml of methanol. The eluate was evaporated and redissolved in 1 ml of 50 mM sodium phosphate buffer, pH 7.4. The obtained *N*^α-[U-¹³C₆, ¹⁵N₂]Fmoc-lysine was modified with 1 mM 2-nonenal for 24 h at 37 °C and subsequently treated with 20% piperidine for 2 h at room temperature to remove the Fmoc moiety. The resulting mixture was purified by HPLC, carried out under the same HPLC conditions as already described. LC/ESI/MS/MS analysis with MRM mode of the isotope-labeled HPH-lysines showed that the standards contained no endogenous (nonlabeled) adducts (supplemental Fig. S1).

LC/ESI/MS/MS—Mass spectrometric analyzes were performed using a Quattro Ultima triple stage quadrupole mass spectrometer (Waters-Micromass, Manchester, UK) equipped with an ESI probe and interfaced with a Shimadzu HPLC system (Shimadzu, Kyoto, Japan). The sample injection volumes of 20 µl each were separated on a Shim-pack VP-ODS 2.0 × 150 mm, 5-µm column (Shimadzu) at a flow rate of 0.3 ml/min. A

discontinuous gradient was used by solvent A (H₂O containing 0.1% formic acid) with solvent B (acetonitrile) as follows: isocratic elution with 20% solvent B from 0 to 5 min; increasing to 50% solvent B from 5 to 20 min; increasing to 70% solvent B from 20 to 25 min; and then isocratic elution with 70% solvent B from 25 to 30 min. Mass spectrometric analyses were performed on line using ESI/MS/MS in the positive ion mode with MRM mode (cone potential 35 eV/collision energy 24 eV). The MRM transitions monitored were as follows: [U-¹³C₆, ¹⁵N₂]HHP-lysine, *m/z* 397 → 261; *cis*- and *trans*-HHP-lysine, *m/z* 389 → 260. L-Glutamate upon reaction with 2-nonenal gave similar MRM transitions but MRM transitions (360 → 260) were detected in the reaction mixture of 2-nonenal/glutamate; however, their elution times were completely different from those of standard HHP-lysines (supplemental Fig. S2). The amount of each HHP-lysine adduct was quantified by the ratio of the peak area of the target adducts and of the HHP-lysine-stable isotope. The HHP-lysine standard concentration was determined by assay of the amino groups using a 2,4,6-trinitrobenzenesulfonic acid assay (16). Briefly, to 30 μl of hydrolyzed HHP-lysine solution was added 30 μl of 4% NaHCO₃ and 30 μl of 0.1% 2,4,6-trinitrobenzenesulfonic acid. The solution was allowed to react at 37 °C for 2 h, and 30 μl of 1% SDS and 15 μl of 1 N HCl were then added. The absorbance of the solution was read at 340 nm. The standard curve (using valine as a standard) was linear in the range 0–3.3 nmol of NH₂. QuanLynx (version 4.0) software (Waters-Micromass) was used to create standard curves (supplemental Fig. S3) and to calculate the adduct concentrations.

For the LC/ESI/MS/MS analysis of the HHP-lysines *in vitro*, the protein samples were treated with an equal volume of 20% trichloroacetic acid. After centrifugation at 5,000 × *g* for 10 min at 4 °C, the proteins were hydrolyzed *in vacuo* with 2 ml of 6 N HCl for 24 h at 110 °C. The internal standard, [U-¹³C₆, ¹⁵N₂]HHP-lysine, was added to the samples prior to the acid hydrolysis. After the acid hydrolysis, the samples were partially separated with Oasis hydrophilic-lipophilic balance (HLB) cartridges (Waters, Milford, MA). After the sample loading, the HLB cartridges were washed with 2 ml of 50% methanol, and the HHP-lysines were eluted with 2 ml of 80% methanol. The samples were then dried, dissolved in methanol, and subjected to LC/ESI/MS/MS analysis.

For the LC/ESI/MS/MS analyses of the HHP-lysines *in vivo*, male ddY mice (Shizuoka Laboratory Animal Center, Shizuoka), weighing 25–35 g (6 weeks of age), were used. Animals received a single intraperitoneal injection of Fe³⁺-NTA (5 mg of iron/kg of body weight). They were sacrificed at 0, 1, 3, 6, and 24 h after the administration. Both kidneys of each animal were immediately removed. The kidneys were homogenized in a Teflon homogenizer in 10 volumes of PBS containing butylated hydroxytoluene (1 mM). The homogenate was centrifuged at 18,000 × *g* for 15 min, and the precipitates were hydrolyzed *in vacuo* with 6 N HCl (2 ml) and [U-¹³C₆, ¹⁵N₂]HHP-lysine for 24 h at 110 °C. The hydrolysates were then dried and dissolved in methanol. After the acid hydrolysis, the samples were partially separated with HLB cartridges and subjected to LC/ESI/MS/MS analysis.

DiD-labeled AcLDL Uptake Assays—DiD (1,1'-dioctadecyl-3,3,3',3'-tetramethylindodicarbocyanine perchlorate)-labeled AcLDL was prepared from human LDL according to the methods previously described for 1,1'-dioctadecyl-3,3,3',3'-tetramethylindodicarbocyanine perchlorate labeling (17). CHO cells that stably expressed CFP-tagged LOX-1 (18) were grown on coverslips. For the cells transiently expressing CFP, CHO cells suspended at a density of 1 × 10⁴ cells/ml were plated on a coverslip 24 h prior to transfection. The cells (40% confluent) were transfected with pECFP-N1 (Clontech) using Lipofectamine reagent according to the manufacturer's protocol and then incubated for 48 h. Cells were treated with each concentration of adducts prepared in F-12 medium without fetal calf serum for 10 min at 37 °C in a 5% CO₂ humidified atmosphere, followed by incubation with DiD-AcLDL (0.4 μg/coverslip) for another 15 min. The cells were then fixed with 2% formaldehyde. Each coverslip was inverted onto a glass slide with a spacer, and the cells were examined using a Leica DM IRE2 microscope (Leica Microsystems, Wetzlar, Germany) equipped with a ×100, NA 1.4 objective and a Cool SNAP-HG digitalized cooled CCD camera (Roper Scientific, Trenton, NJ) driven by MetaMorph software (Universal Imaging, Downingtown, PA). The expression level of LOX-1 was examined by the CFP fluorescence intensity using an E4 filter with excitation at 436 nm (7-nm bandpass) and a 470-nm long pass emission filter. Images were acquired at 0.2 s exposure time. The DiD-AcLDL uptake was analyzed by the amount of the DiD-derived fluorescence intensity using a Y5 filter, with excitation using a 620 nm (50-nm bandpass) and 700 nm (75-nm bandpass) emission filters. The images were acquired at a 2-s exposure.

Images of over 100 cells from three independent experiments were acquired. After subtracting the background emission level with respect to 436 and 620 nm from the fluorescence image, the fluorescence intensity of each cell was determined from the average pixel value of the whole cell. The expression level of LOX-1 was calculated from the CFP intensity, and the level of uptake of AcLDL was calculated from the DiD intensity (18). For each experimental condition, the level of AcLDL uptake was averaged per expression level of LOX-1.

RESULTS

Monoclonal Antibody against Protein-bound 2-Nonenal—To assess the reactivity of 2-nonenal to proteins, HSA (1 mg/ml) was exposed to 2-nonenal (0–10 mM) under physiological conditions *in vitro*, and changes in the amino acid composition of the protein were examined by an amino acid analysis. As shown in Fig. 1B, 2-nonenal preferentially reacted with the lysine residues, indicating that 2-nonenal can covalently modify protein spontaneously, and the likely mechanism is a nucleophilic attack by the protein.

To determine whether modification of proteins by 2-nonenal occurs *in vivo*, we attempted to develop a mAb against 2-nonenal-modified protein. To this end, the keyhole limpet hemocyanin that had been exposed to 2-nonenal was administered to mice at 10-day intervals. During the preparation of the mAb, hybridomas were selected by comparing the reactivities of the culture supernatant to the 2-nonenal-modified BSA. Among the four obtained clones, the clone 27Q4 showed the most dis-

Lipid Peroxidation Generates Protein-bound 2-Nonenal

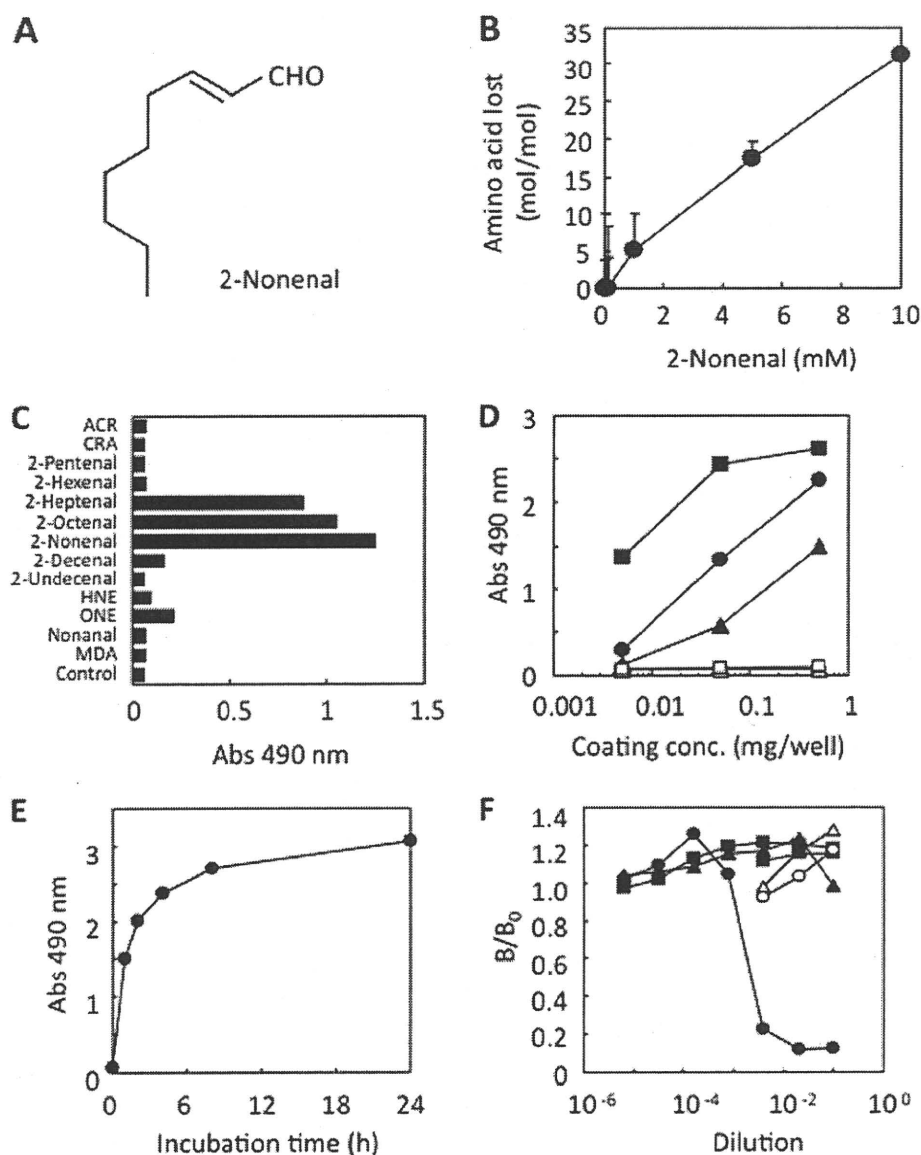


FIGURE 1. Monoclonal antibody against protein-bound 2-nonenal. *A*, chemical structure of 2-nonenal. *B*, loss of lysine residues in protein treated with 2-nonenal. HSA (1 mg/ml) was incubated with 0–10 mM 2-nonenal in 50 mM sodium phosphate buffer, pH 7.2, at 37 °C. *C*, immunoreactivity of mAb 27Q4 to aldehyde-modified proteins. A coating antigen (0.5 μ g/well) was prepared by incubating 1 mg of BSA with 1 mM aldehydes in 1 ml of 50 mM sodium phosphate buffer, pH 7.2, for 24 h at 37 °C. ACR, acrolein; CRA, crotonaldehyde; MDA, malondialdehyde; HNE, 4-hydroxy-2-nonenal; ONE, 4-oxo-2-nonenal. *D*, immunoreactivity of mAb 27Q4 to 2-nonenal-modified proteins. A coating antigen (0.005–0.5 μ g/well) was prepared by incubating 1 mg of protein with 1 mM 2-nonenal in 1 ml of 50 mM sodium phosphate buffer, pH 7.2, for 24 h at 37 °C. Proteins are as follows: open square, native lactoglobulin; closed triangle, 2-nonenal-modified HSA; closed circle, 2-nonenal-modified BSA; closed square, 2-nonenal-modified lactoglobulin. *E*, time-dependent increase in the immunoreactivity of protein treated with 2-nonenal. HSA (1 mg/ml) was incubated with 1 mM 2-nonenal in 50 mM sodium phosphate buffer, pH 7.2, at 37 °C. *F*, competitive ELISA analysis with the reaction mixtures of amino acid derivatives and 2-nonenal. Competitors were prepared by incubating 50 mM amino acid derivatives, *N*^ε-acetyllysine, *N*^ε-acetylhistidine, or *N*^ε-acetylcysteine, in the presence or absence of 2-nonenal (50 mM), in 50 mM sodium phosphate buffer, pH 7.2, for 24 h at 37 °C. Competitors are as follows: open circle, *N*^ε-acetyllysine; open triangle, *N*^ε-acetylhistidine; open square, *N*^ε-acetylcysteine; closed circle, 2-nonenal/*N*^ε-acetyllysine; closed triangle, 2-nonenal/*N*^ε-acetylhistidine; closed square, 2-nonenal/*N*^ε-acetylcysteine.

tinctive recognition of the 2-nonenal-modified BSA. The specificity of the obtained antibody was characterized. As shown in Fig. 1C, the monoclonal antibody showed a strong immunoreactivity not only with 2-nonenal but also with 2-octenal and 2-heptenal, whereas the unmodified BSA was not recognized by

the antibody. We then determined whether the 2-nonenal-modified proteins contained the 27Q4 epitope. The mAb 27Q4 immunoreacted with not only 2-nonenal/BSA, but also with 2-nonenal/HSA and 2-nonenal/lactoglobulin, whereas the unmodified proteins were not recognized by the antibody (Fig. 1D), suggesting that the 2-nonenal-modified proteins contained a common adduct structure recognized by mAb 27Q4. The time course study of formation of the 2-nonenal epitope during the incubation of BSA with 2-nonenal *in vitro* was determined by direct ELISA using mAb 27Q4. When BSA was incubated with 1 mM 2-nonenal at 37 °C, the immunoreactive materials rapidly increased within 4 h (Fig. 1E). To identify the possible attacking nucleophiles that form antigenic structures, we investigated the reaction of 2-nonenal with individual amino acids likely to form stable antigenic products. We studied lysine, histidine, and cysteine, each protected at the α -amino group as an acetamide, leaving only the side-chain nucleophile as a potential reactant. As shown in Fig. 1F, binding of the 2-nonenal-modified protein to the antibody was hardly inhibited by the reaction mixtures of 2-nonenal/histidine and 2-nonenal/cysteine but was significantly inhibited by the reaction mixture of 2-nonenal/lysine, suggesting that the mAb might recognize a 2-nonenal-lysine adduct as the epitope. None of the original amino acid derivatives, histidine, cysteine, and lysine, cross-reacted with mAb 27Q4.

Isolation and Structural Characterization of the Antigenic 2-Nonenal-Lysine Adducts—Because characterization of the ability of antibodies to recognize specific molecular targets in their native three-dimensional conformation is critical to the use of these reagents,

we sought to identify the intrinsic epitope recognized by mAb 27Q4. To identify the 2-nonenal-lysine adduct recognized by mAb 27Q4, the immunoreactivity with the reaction products of 2-nonenal with *N*^ε-acetyllysine was characterized. As shown in Fig. 2A, the ELISA analysis of the HPLC fractions for immuno-

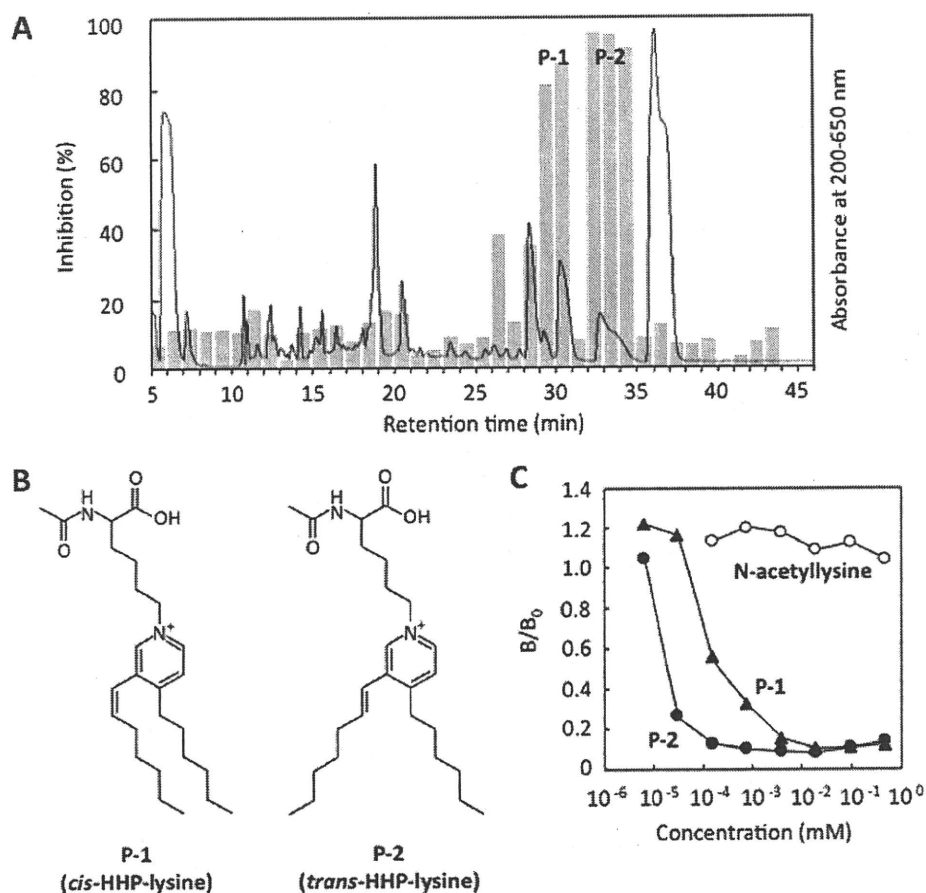


FIGURE 2. Isolation and structural characterization of the antigenic 2-nonenal-lysine adducts. **A**, competitive ELISA analysis of HPLC fractions for immunoreactivity with mAb 27Q4. The reaction was performed by incubating 200 mM N^{α} -acetyllysine with 200 mM 2-nonenal in 1 ml of 50 mM sodium phosphate buffer, pH 7.2, at 37 °C for 24 h. Solid line, profile of UV absorbance at 200–650 nm. Bar, competitive ELISA analysis. **B**, chemical structures of *cis*-HHP-lysine and (P-1) and *trans*-HHP-lysine (P-2). **C**, competitive ELISA analysis with *cis*- and *trans*-HHP-lysine. Competitors are as follows: closed circle, N^{α} -acetyl-*trans*-HHP-lysine (P-2); closed triangle, N^{α} -acetyl-*cis*-HHP-lysine (P-1); open circle, N^{α} -acetyllysine.

reactivity with mAb 27Q4 showed that the antibody primarily had an immunoreactivity with two fractions, P-1 and P-2. The LC/MS total ion current analysis of P-2 detected one product, which showed a 242-Da increase in the mass value of the unmodified lysine derivative and gave the $[M + H]^+$ peak at m/z 431.0 (supplemental Fig. S4), suggesting that it was composed of one molecule of N^{α} -acetyllysine and two molecules of 2-nonenal.

Because P-2 was a major immunoreactive fraction, we first attempted to identify this product. To characterize the chemical structure, isolation by HPLC on the reverse-phase column was carried out. After purification, the structure of the products was characterized by an NMR analysis. The assignments of protons and carbons were based on the result of the HMBC and distortionless enhancement by polarization transfer experiments. Compared with the ^{13}C NMR and ^1H NMR spectra between N^{α} -acetyllysine and the product (supplemental Figs. S5–S10), the Cb (173.3 ppm), the Cd (175.1 ppm), the Ha proton (1.96 ppm), and the Hc proton (δH 4.39 ppm; δC 53.0 ppm) remained in the ^{13}C NMR and ^1H NMR spectra of the product. The correlation spectroscopy spectrum showed correlations between the Hc proton with the He (δH 1.70–1.92 ppm; δC 32.1 ppm) proton, the He proton with the Hf proton (δH 1.40–

1.52 ppm; δC 23.4 or 23.5 ppm), the Hf proton with the Hg proton (δH 2.01–2.06 ppm; δC 31.6 ppm), and the Hg proton with the Hh proton (δH 4.53 ppm; δC 62.0 ppm). The ^{13}C NMR spectrum of the product showed five signals (δC 129.2, 139.4, 142.2 (two carbon signals), and 160.7 ppm) in the aromatic carbon region. In the HMBC spectrum, cross-peaks between the δ -proton of the lysine residue, Hh, and carbons (Hh-Ci (142.2 ppm) and Hh-Cm (142.2 ppm)), cross-peaks between Hi (8.61 ppm, $J = 6.0$ Hz) and carbons (Hi-Ch, Hi-Cj (129.2 ppm) and Hi-Ck (160.7 ppm)), and cross-peaks between Hm (8.91 ppm) with carbons (Hm-Ch, Hm-Ci, Hm-Ck, and Hm-Cl (139.4 ppm)). The coupling constant and HMBC spectrum indicated that Hi and Hj (7.84 ppm, $J = 6.0$ Hz) are adjacent. Moreover, in the HMBC spectrum, the cross-peaks Hj and carbons (Hj-Ci, Hj-Ck, and Hj-Cl) are observed. The Ck and Cl were missing from the distortionless enhancement by polarization transfer spectrum. This indicates that Ck and Cl are quaternary carbons. These results suggest that the aromatic part of this product seemed to be a pyridinium ring, in which Ck and Cl are substituted. The coupling constant for the vinyl proton (Ht,

6.66 ppm) was $J = 16.2$ Hz for the *trans*-proton. In the HMBC spectrum, the cross-peaks between the Ht and carbons (Ht-Ck, Ht-Cl, and Ht-Cm) and cross-peaks between the Hn and carbons (Hn-Cj, Hn-Ck, and Hn-Cl) were observed. These results indicated that the substituted quaternary carbons, Ck and Cl, were adjacent to Cn and Ct, respectively. The residual parts of P-2 were the (*E*)-1-heptenyl and hexyl groups. The signals at 0.89–0.94 ppm were assigned to Hs and Hz. The correlation spectroscopy experiments were performed to determine the alkyl chain connectivity. With the correlation spectroscopy spectrum, starting from the methyl groups, the spin systems for an (*E*)-1-heptenyl chain and a hexyl chain were determined. After establishing the connectivities for the alkyl chains, the HMBC experiments were performed. Based on these characteristics, it was determined that P-2 was the novel 2-nonenal-lysine adduct, N^{α} -acetyl- N^{ϵ} -3-[(hept-1-enyl)-4-hexylpyridinium]lysine (N^{α} -acetyl-HHP-lysine) (Fig. 2B). The LC/MS total ion current analysis of P-1 detected one product, which showed a 242-Da increase in the mass value of the unmodified lysine derivative and gave the $[M + H]^+$ peak at m/z 430.9 (supplemental Fig. S11), suggesting that P-1 is a *cis* isomer of N^{α} -acetyl-HHP-lysine. To confirm the structure of P-1, the

Lipid Peroxidation Generates Protein-bound 2-Nonenal

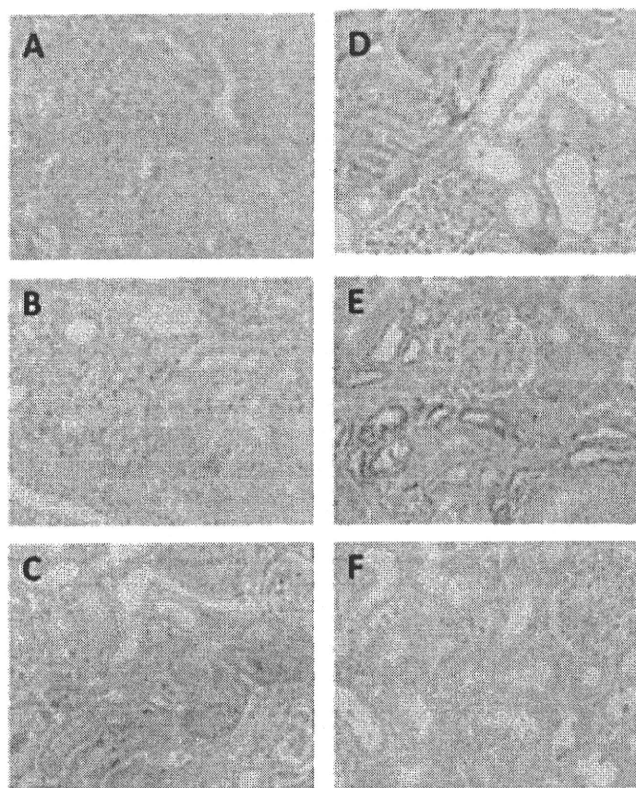


FIGURE 3. Immunohistochemistry of renal cortex with mAb 27Q4 ($\times 400$). A, untreated control; B, 1 h; C, 6 h; D, 24 h; E, 48 h after single intraperitoneal injection of Fe^{3+} -NTA; F, 3 weeks after repeated intraperitoneal injection of Fe^{3+} -NTA. Refer to "Experimental Procedures" for details.

NMR experiments were performed (supplemental Figs. S12–S17) and showed that the coupling constant for the vinyl proton (6.51 ppm) was $J = 11.6$ Hz for the *cis* proton. Selected ion-current chromatograms obtained from the LC/MS analysis showed that, when 200 mM N^{α} -acetyllysine was incubated with 200 mM 2-nonenal for 72 h, P-1 and P-2 were formed in the ratio of 1:1.4, indicating that the *cis* isomer of N^{α} -acetyl-HHP-lysine can be formed from the *trans*-2-nonenal-mediated reaction.

As shown in Fig. 2C, the antibody showed a specificity toward both P-1 and P-2 but was rather specific to P-2. Approximately 50 pmol of P-2/well (100 μl) caused a 50% inhibition of the antibody binding to the 2-nonenal-modified protein, whereas at least 100-fold higher concentrations of P-1 were necessary for the same inhibition.

Formation of Immunoreactive Materials with mAb 27Q4 in Vivo—We next sought to explore whether immunoreactive materials with mAb 27Q4 are formed *in vivo*. For this purpose, we used Fe^{3+} -NTA-treated rats, an established animal model of oxidant injury to the kidney. It has been established that Fe^{3+} -NTA induces acute renal proximal tubular necrosis, a consequence of oxidative tissue damage, that eventually leads to a high incidence of renal adenocarcinoma in rodents (11). Previously, we have shown that the levels of 2-nonenal markedly increase after the administration of Fe^{3+} -NTA (5). In the control rat kidney (Fig. 3A), an almost negligible level of immunoreactivity was observed. The immunoreactivities were found

in some of the renal proximal tubular cells 1, 6, 24, and 48 h (Fig. 3, B–E) after the administration of 15 mg of iron/kg of body weight of Fe^{3+} -NTA. No immunoreactivity was observed after the repeated (3 weeks) administrations of Fe^{3+} -NTA (Fig. 3F). These patterns of distribution in the rat kidney are consistent with those of the distribution of membrane lipid peroxidation products and their conjugates with cytosolic proteins, suggesting a correlation between the production of the 2-nonenal/2-alkenals and oxidative stress. Pre-absorption of the antibody with HHP-lysine completely abolished the immunostaining (data not shown).

LC/ESI/MS/MS Analysis of HHP-lysine—To obtain direct evidence for the formation of the antigenic HHP-lysine adducts *in vivo*, we first attempted to establish a method for the detection of adducts using LC/ESI/MS/MS. The acid hydrolysis of N^{α} -acetyl-HHP-lysine gave a single product, which was identified to be the expected de-acetylated product (HHP-lysine) (supplemental Figs. S18 and S19). Collision-induced dissociation of the HHP-lysine produced relevant daughter ions at m/z 344, 260, 130, and 84 (Fig. 4A). These ions were applied to the structure shown in Fig. 4B. The product ions at m/z 84 and 130 were confirmed to be the product ions of a lysine moiety, and the ions at m/z 344 and 389 originated from the HHP-lysine. Fig. 4C demonstrates the LC/ESI/MS/MS analysis of the HHP-lysine (0–10 nM) in the positive ion mode using MRM between the transition from the protonated parent ion $[M + H]^+$ to the characteristic daughter ion (m/z 389.6 \rightarrow 260.2), allowing detection of both the *cis*- and *trans*-HHP-lysines. Chromatograms for the internal standard are shown in supplemental Fig. S20. Using the LC/ESI/MS/MS technique, we attempted to detect HHP-lysine in the 2-nonenal-modified HSA. No adducts were detected in the native HSA, whereas the treatment of HSA with 0–10 mM 2-nonenal in 50 mM sodium phosphate buffer, pH 7.2, for 24 h at 37 $^{\circ}\text{C}$ gave 0.61 and 0.86 mol of the *cis*- and *trans*-HHP-lysines, respectively, per mol of protein (Fig. 4, D and E).

In Vivo Formation of HHP-lysine via Lipid Peroxidation—It is known that 2-nonenal is generated by the lipid peroxidation of unsaturated fatty acids, such as palmitoleic acid (6). To examine the involvement of the lipid peroxidation during the formation of HHP-lysine, we sought to detect HHP-lysine in the Cu^{2+} -oxidized LDL using LC/ESI/MS/MS. Incubation of LDL with Cu^{2+} led to the oxidation of the LDL as assessed by the formation of thiobarbituric acid-reactive substances (data not shown). As shown in Fig. 5A, the Cu^{2+} -induced peroxidation of LDL dramatically enhanced the formation of HHP-lysine with the levels of the *trans*-HHP-lysine exceeding those of the *cis*-HHP-lysine by 2-fold.

To further examine which fatty acids are involved in the formation of the HHP-lysine, several unsaturated fatty acids were incubated with an iron/ascorbate-mediated free radical generating system in the presence of HSA, and HHP-lysine generated on the protein molecule was analyzed by LC/ESI/MS/MS following acid hydrolysis. As shown in Fig. 5B, the iron/ascorbate-mediated oxidation of palmitoleic acid and $\omega 6$ -polyunsaturated fatty acids, such as linoleic acid, γ -linolenic acid, and arachidonic acid, in the presence of HSA resulted in a dramatic

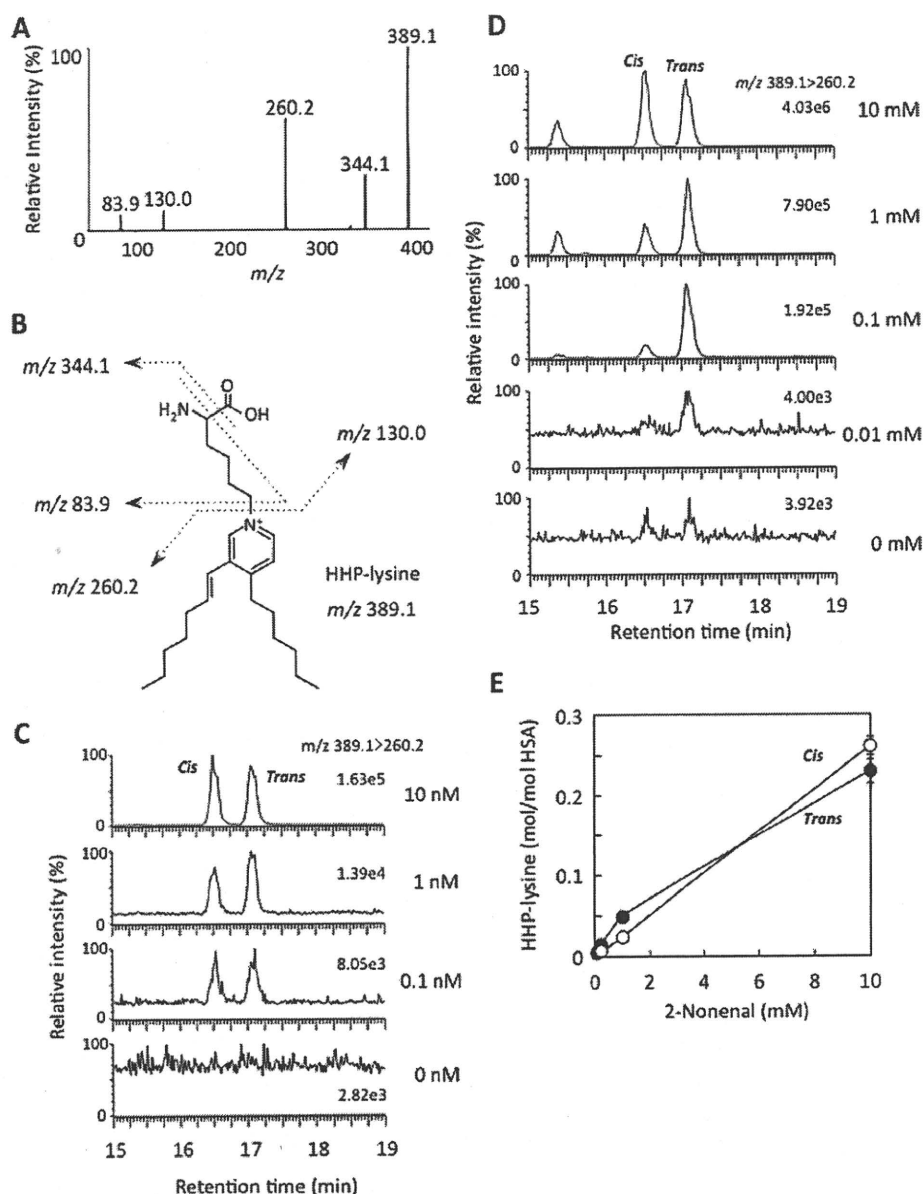


FIGURE 4. LC/ESI/MS/MS analysis of HHP-lysine. *A*, collision-induced dissociation of the $[M + H]^+$ of *trans*-HHP-lysine at m/z 389.5 at a collision energy of 25 V. *B*, proposed structures of individual ions. *C*, LC/ESI/MS/MS analysis of authentic *cis*- and *trans*-HHP-lysines. The ion current tracing of HHP-lysine using LC/ESI/MS/MS with MRM is shown. *D*, LC/ESI/MS/MS analysis of *cis*- and *trans*-HHP-lysines using LC/ESI/MS/MS with MRM is shown. *E*, dose-dependent formation of *cis*- and *trans*-HHP-lysines in the 2-nonenal-modified HSA. Symbols used are as follows: open circle, *cis*-HHP-lysine; closed circle, *trans*-HHP-lysine. *D* and *E*, HSA (1.0 mg/ml) was incubated with 2-nonenal (0–10 mM) in 50 mM sodium phosphate buffer, pH 7.2, for 24 h at 37 °C. The native and modified HSA were analyzed by LC/ESI/MS/MS with MRM mode followed by acid hydrolysis.

increase in the levels of HHP-lysine with levels of *trans*-HHP-lysine exceeding those of *cis*-HHP-lysine by 3–9-fold.

We then sought to explore whether HHP-lysine is formed in the kidney of animals exposed to Fe^{3+} -NTA *in vivo*. Kidneys from the untreated and treated animals collected 1 and 3 h after the administration of Fe^{3+} -NTA were analyzed for HHP-lysine using LC/ESI/MS/MS. The MRM transitions monitored were as follows: $[U-^{13}C_6, ^{15}N_2]$ HHP-lysine, m/z 397 \rightarrow 261; *cis*- and *trans*-HHP-lysine, m/z 389 \rightarrow 260. Multiple distinct MRM channels (parent 389.1 \rightarrow 344.1, 260.2, 130.0, and 83.9) showed

that each of the appropriate transitions showed co-chromatography (supplemental Figs. S21 and S22). In addition, the ratio of the different parent \rightarrow daughter transitions was also checked (Fig. 5C). As shown in Fig. 5D, the levels of both the *cis*- and *trans*-HHP-lysines markedly increased 3 h after the administration of Fe^{3+} -NTA. The yields of the *cis*- and *trans*-HHP-lysines at 3 h were 366.5 and 357.8 fmol/g wet tissue weight, respectively.

Recognition of the 2-Nonenal-Lysine Adduct by LOX-1—Finally, we evaluated the biological implication of the 2-nonenal modification of protein. To this end, based on the previous findings that a scavenger receptor LOX-1 might be involved in the processing of aldehyde-modified proteins (19) and that, among the aldehyde-treated proteins, the 2-nonenal-modified protein can be very efficiently incorporated into the LOX-1-overexpressing cells,³ we sought to examine if LOX-1 recognizes the 2-nonenal-lysine adduct. AcLDL was used as an alternative ligand to the oxidized LDL, which shows a comparable affinity to LOX-1 (20) to avoid ambiguous effects from variations in the extent of the oxidized LDL oxidation (21, 22). In this assay, the amount of incorporated DiD-labeled AcLDL directly reflected the binding activity of LOX-1, which was confirmed by an independent analysis as described previously (23). The rate of DiD-AcLDL taken up by CHO stably expressing CFP/LOX-1 was assessed by a fluorescence microscope equipped with a cooled CCD camera. In CHO cells transfected with pECFP-N1, the CFP signal was detected in the cytoplasm, and no DiD-AcLDL uptake was detected

(Fig. 6A, top). The stable cell line expressed a moderate amount of LOX-1, and a fluorescence derived from DiD-AcLDL was observed (Fig. 6A, middle). The effect of the 2-nonenal-modified BSA upon DiD-AcLDL uptake through LOX-1 was examined in the competition assay to evaluate the LOX-1 recognition of modified proteins. The native BSA failed to show any inhibitory effects (date not shown), whereas the protein modi-

³ S. Machida and K. Uchida, manuscript in preparation.

Lipid Peroxidation Generates Protein-bound 2-Nonenal

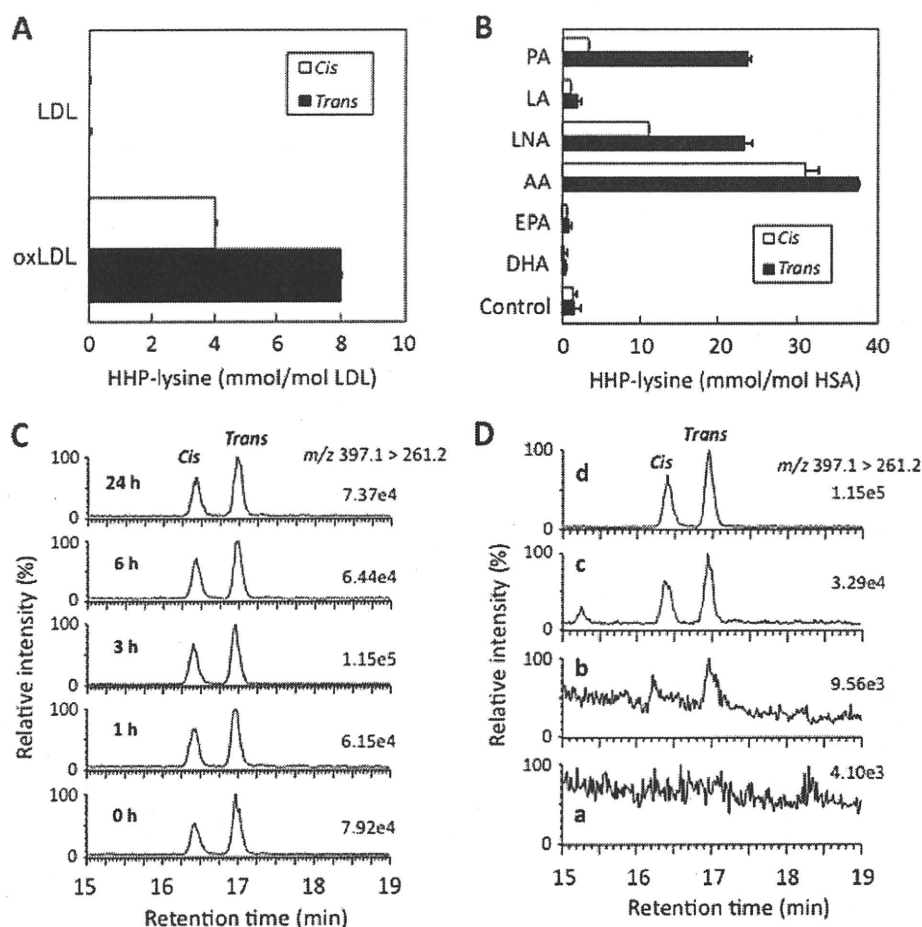


FIGURE 5. *In vivo* formation of HHP-lysine via lipid peroxidation. *A*, LC/ESI/MS/MS analysis of *cis*- and *trans*-HHP-lysines in oxidized LDL (*oxLDL*). LDL (0.5 mg) was incubated with 5 μM Cu^{2+} in 1 ml of PBS at 37 $^{\circ}\text{C}$. The native LDL and oxidized LDL were analyzed by LC/ESI/MS/MS with MRM mode followed by acid hydrolysis. *B*, LC/ESI/MS/MS analysis of *cis*- and *trans*-HHP-lysines in protein exposed to lipid peroxidation. The metal-catalyzed oxidation of unsaturated fatty acids in the presence of HSA was performed by incubating HSA (1 mg/ml) with 2 mM unsaturated fatty acids in the presence of 50 μM Fe^{2+} and 1 mM ascorbic acid in 1 ml of 50 mM sodium phosphate buffer, pH 7.2, in atmospheric oxygen at 37 $^{\circ}\text{C}$. The native and modified HSA were analyzed by LC/ESI/MS/MS with MRM mode followed by acid hydrolysis. The abbreviations used are as follows: PA, palmitoleic acid; LA, linoleic acid; LNA, γ -linolenic acid; AA, arachidonic acid; EPA, eicosapentaenoic acid; DHA, docosahexaenoic acid. *C*, LC/ESI/MS/MS analysis of *cis*-[$U\text{-}^{13}\text{C}_6, ^{15}\text{N}_2$]- and *trans*-[$U\text{-}^{13}\text{C}_6, ^{15}\text{N}_2$]-HHP-lysines in the kidneys of mice exposed to Fe^{3+} -NTA. The ion current tracing of *cis*-[$U\text{-}^{13}\text{C}_6, ^{15}\text{N}_2$]- and *trans*-[$U\text{-}^{13}\text{C}_6, ^{15}\text{N}_2$]-HHP-lysines LC/ESI/MS/MS with MRM is shown. *D*, LC/ESI/MS/MS analysis of *cis*- and *trans*-HHP-lysines in the kidneys of mice exposed to Fe^{3+} -NTA. The ion current tracing of HHP-lysine using LC/ESI/MS/MS with MRM is shown. Panel *a*, 0 h after administration; panel *b*, 1 h after administration; panel *c*, 3 h after administration; panel *d*, internal standards.

fied with 2-nonenal significantly inhibited the uptake of AcLDL (Fig. 6A, bottom). Finally, we evaluated the purified *cis*- and *trans*-HHP-lysines for their recognition by LOX-1 in the competition assay, and we observed that they served as a ligand for LOX-1, as evidenced by their ability to effectively compete with AcLDL (Fig. 6, B–D). There was no effect by the 1% DMSO carried from the stock solution of the HHP-lysine (data not shown).

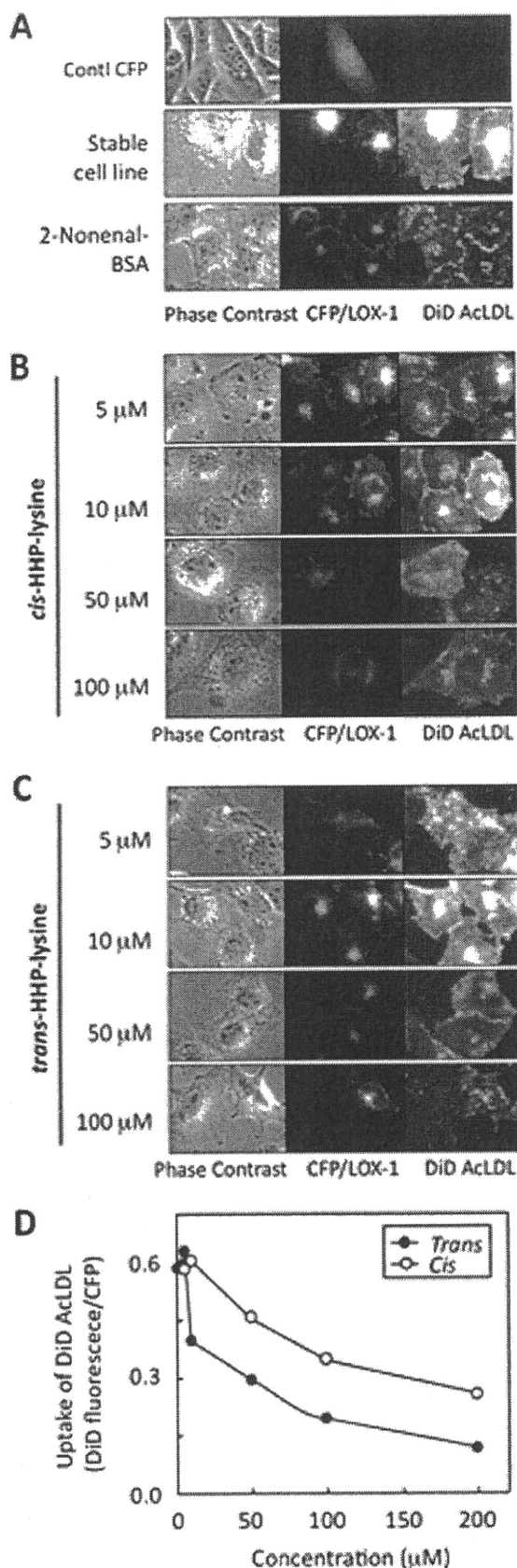
DISCUSSION

Lipid peroxidation proceeds by a free radical chain reaction mechanism and yields lipid hydroperoxides as major initial reaction products. Subsequently, the decomposition of the lipid hydroperoxides generates a number of breakdown products that display a wide variety of damaging actions. A number of

reactive aldehydes derived from lipid peroxidation have been implicated as causative agents in cytotoxic processes initiated by the exposure of biological systems to oxidizing agents (2). On the basis of a large number of reports concerning the detection of lipid peroxidation-specific adducts as biomarkers in human diseases, there is no doubt that the steady-state levels of lipid peroxidation products increase in pathophysiological states associated with oxidative stress. Considerable progress has also recently been made toward understanding the mechanisms of action of lipid peroxidation products. The quantitative and analytical importance of lipid peroxidation-specific adducts has prompted the development of methods to specifically analyze these adducts to understand their chemical nature, formation pathway, and distribution level *in vivo*.

The results presented herein show that 2-nonenal, a body odorant originating from lipid peroxidation, covalently modifies proteins. A spontaneous chemical reaction was observed *in vitro*. In addition, we obtained a murine monoclonal antibody, mAb 27Q4, that clearly distinguished the 2-nonenal-modified protein from the native protein. This antibody appeared to be highly specific for the protein-bound 2-alkenals, including 2-heptenal, 2-octenal, and 2-nonenal. Using the antibody, the formation of the 2-nonenal-modified proteins *in vivo* was tested in the kidney of rats exposed to Fe^{3+} -NTA. The iron

chelate was originally used for an experimental model of iron overload (24). Repeated intraperitoneal injections of Fe^{3+} -NTA were reported to induce acute and subacute renal proximal tubular necrosis and a subsequent high incidence (60–92%) of renal adenocarcinoma in male rats and mice (25, 26). A single injection of Fe^{3+} -NTA causes a number of time-dependent morphological alterations in the structure and the function of the renal proximal tubular cells and their mitochondria. During the early stage of injury, typical cellular changes are the loss of the brush border, cytoplasmic vesicles, mitochondrial disorganization, and dense cytoplasmic deposits in the proximal tubular cells. Most of the damaged epithelia show the typical appearance of necrotic cells, and more than half of the proximal tubular cells are gone. It has been suggested that oxidative stress is one of the basic mechanisms of Fe^{3+} -NTA-in-



duced acute renal injury and is closely associated with renal carcinogenesis (27, 28). The present *in vivo* study has shown that lipid peroxidation generates 2-nonenal covalently bound to proteins in the renal proximal tubules of rats treated with Fe^{3+} -NTA (Fig. 3). To the best of our knowledge, this is the first report of the *in vivo* formation of protein-bound 2-nonenal/2-alkenals in the target organ of the carcinogenic protocol. It was also striking that the immunoreactivities with mAb 27Q4 were detected even 48 h after the administration of Fe^{3+} -NTA (Fig. 3E). Long retention of this aldehyde may play a role in the Fe^{3+} -NTA-induced renal carcinogenesis.

Upon investigation of an antigenic adduct recognized by the antibody (mAb 27Q4), we unexpectedly identified novel lysine-pyridinium adducts, *cis*- and *trans*-HHP-lysines. Of interest, the monoclonal antibodies raised against protein-bound 2-alkenals, such as acrolein and crotonaldehyde, recognize pyridinium-containing adducts as the major epitopes (29, 30). It is likely that, due to the placement of a fixed, positive charge on the ϵ -amino group, the pyridinium-containing adducts could be an important immunological epitope generated in 2-alkenal-modified proteins. The formation of the 3,4-substituted pyridinium adducts has also been reported to be a dominant pathway for modification of the primary amine with 2-alkenals, such as 2-hexenal and 2-octenal (31, 32). Based on these studies, HHP-lysine is likely to be formed through the formation of the 2-nonenal-lysine Schiff base (Fig. 7). After the formation of the Schiff base adduct, the C3 position of the initial Schiff base may be attacked by the C2 of the enolate anion from the second aldehyde, followed by dehydration and cyclization to form the isomeric pyridinium adduct. On the other hand, *trans-cis* isomerization of α,β -unsaturated compounds is known to be catalyzed by amines (addition-elimination). Thus, the isomerization required for the formation of *cis*-HHP-lysine may occur at the stage of the free 2-nonenal or following Schiff base formation.

Due to the fact that the core structures of the pyridinium-containing lysine adducts are resistant to the conventional acid hydrolysis of proteins, we established a highly sensitive method for the detection of *cis*- and *trans*-HHP-lysine using LC/ESI/MS/MS. *In vitro* studies of the detection of HHP-lysine demonstrated that the 2-nonenal-lysine adducts were generated in the oxidized LDL (Fig. 5A). In addition, substantial amounts of the 2-nonenal-lysine adducts, mainly the *trans*-HHP-lysine, were detected in the metal-catalyzed peroxidation of unsaturated

FIGURE 6. Effect of the 2-nonenal-lysine adducts on ligand uptake by LOX-1. A, CHO cells transfected with vector carrying only CFP (top). LOX-1 expression level and AcLDL uptake ability of stable cell line (middle) is shown. Effect of 2-nonenal-modified BSA (4 $\mu\text{g}/\text{ml}$) on AcLDL uptake (bottom) is shown. B, effect of *cis*-HHP-lysine (10–100 μM) on AcLDL uptake. C, effect of *trans*-HHP-lysine (10–100 μM) on AcLDL uptake. Images were acquired using $\times 100$ objective. Panels are as follows: left, phase contrast; middle, CFP/LOX-1 (excitation at 436 nm; exposure time, 0.2 s); right, DiD-AcLDL (excitation at 620 nm; exposure time, 2 s). D, quantitative measurement of fluorescence intensity of each cell. CHO cells stably expressing CFP/LOX-1 were treated with each concentration of adducts and followed by incubation with DiD-AcLDL. The cell-associated fluorescence intensity derived from CFP and DiD (pixel value) was determined as described under "Experimental Procedures." The specific uptake was expressed as the fluorescence intensity derived from DiD (pixel value) per the fluorescence intensity derived from CFP (pixel value) of each cell. The values represent the means of over 100 cells from three independent experiments.

Lipid Peroxidation Generates Protein-bound 2-Nonenal

- Komba, S., and Machida, S. (2007) *Exp. Cell Res.* **313**, 1203–1214
19. Duryee, M. J., Klassen, L. W., Freeman, T. L., Willis, M. S., Tuma, D. J., and Thiele, G. M. (2003) *Biochem. Pharmacol.* **66**, 1045–1054
20. Shi, X., Niimi, S., Ohtani, T., and Machida, S. (2001) *J. Cell Sci.* **114**, 1273–1282
21. Loughheed, M., and Steinbrecher, U. P. (1996) *J. Biol. Chem.* **271**, 11798–11805
22. Yoshida, H., Kondratenko, N., Green, S., Steinberg, D., and Quehenberger, O. (1998) *Biochem. J.* **334**, 9–13
23. Chen, M., Nagase, M., Fujita, T., Narumiya, S., Masaki, T., and Sawamura, T. (2001) *Biochem. Biophys. Res. Commun.* **287**, 962–968
24. Awai, M., Narasaki, M., Yamanoi, Y., and Seno, S. (1979) *Am. J. Pathol.* **95**, 663–673
25. Ebina, Y., Okada, S., Hamazaki, S., Ogino, F., Li, J. L., and Midorikawa, O. (1986) *J. Natl. Cancer Inst.* **76**, 107–113
26. Li, J. L., Okada, S., Hamazaki, S., Ebina, Y., and Midorikawa, O. (1987) *Cancer Res.* **47**, 1867–1869
27. Toyokuni, S. (1996) *Free Radic. Biol. Med.* **20**, 553–566
28. Toyokuni, S. (2009) *Cancer Sci.* **100**, 9–16
29. Furuhashi, A., Ishii, T., Kumazawa, S., Yamada, T., Nakayama, T., and Uchida, K. (2003) *J. Biol. Chem.* **278**, 48658–48665
30. Ichihashi, K., Osawa, T., Toyokuni, S., and Uchida, K. (2001) *J. Biol. Chem.* **276**, 23903–23913
31. Baker, A., Zidek, L., Wiesler, D., Chmelik, J., Pagel, M., and Novotny, M. V. (1998) *Chem. Res. Toxicol.* **11**, 730–740
32. Alaiz, M., and Barragan, S. (1995) *Chem. Phys. Lipids* **77**, 217–223
33. Brown, M. S., Basu, S. K., Falck, J. R., Ho, Y. K., and Goldstein, J. L. (1980) *J. Supramol. Struct.* **13**, 67–81
34. Horiuchi, S., Murakami, M., Takata, K., and Morino, Y. (1986) *J. Biol. Chem.* **261**, 4962–4966
35. Takata, K., Horiuchi, S., Araki, N., Shiga, M., Saitoh, M., and Morino, Y. (1988) *J. Biol. Chem.* **263**, 14819–14825
36. Takata, K., Horiuchi, S., Araki, N., Shiga, M., Saitoh, M., and Morino, Y. (1989) *Biochim. Biophys. Acta* **986**, 18–26
37. Steinbrecher, U. P., Loughheed, M., Kwan, W. C., and Dirks, M. (1989) *J. Biol. Chem.* **264**, 15216–15223
38. Duryee, M. J., Freeman, T. L., Willis, M. S., Hunter, C. D., Hamilton, B. C., 3rd, Suzuki, H., Tuma, D. J., Klassen, L. W., and Thiele, G. M. (2005) *Mol. Pharmacol.* **68**, 1423–1430

